Investigation of carbon dioxide (CO2) capture in a falling film contactor by computer simulation

Saba A. Gheni, Mohammed F. Abed, Essam K. Halabia, Saad R. Ahmed

Oil & Gas Science and Technology - Rev. IFP Energies nouvelles **73**, 43 (2018)

https://doi.org/10.2516/ogst/2018020

Available online at:
www.ogst.ifpenergiesnouvelles.fr

REGULAR ARTICLE OPEN ACCESS

Investigation of carbon dioxide (CO_2) capture in a falling film contactor by computer simulation

Saba A. Gheni[1,*], Mohammed F. Abed[2], Essam K. Halabia[2], and Saad R. Ahmed[3]

[1] Department of Chemical Engineering, University of Missouri, Columbia, MO, USA
[2] Department of Chemical Engineering, University of Technology, Iraq
[3] Department of Mechanical Engineering, University of Tikrit, Iraq

Received: 9 September 2017 / Accepted: 30 April 2018

Abstract. In this work, mathematical models of carbon dioxide (CO_2) absorption by monoethanolamine amine (MEA) in a falling film contactor are developed. The proposed models aim to predict conversion of the gas–liquid reaction along the contactor, gas–liquid interface temperature profile (axial and radial), liquid film thickness along the contactor length, axial and radial concentration profiles of reactants in liquid film, and axial and radial profiles of velocity in the liquid film. A code written in MatLab was used to obtain these profiles based on multi grid method through programming of kinetic and thermodynamic equations and physical properties of the absorption system. The mathematical model is validated by an experimental measurement based on absorption of CO_2 gas by MEA solution. Four parameters are studied as independent variables namely, mole fraction of carbon dioxide in gaseous mixture, molar concentration of absorbent (MEA, volumetric flow rate of MEA, and its temperature. It is found that the entrance effect of the falling film contactor is related to axial distance from the contactor entrance exponentially:

$$E = B_0 \exp(-B_1 y)$$

An optimization technique based on minimization of the sum of the squared error between the experimental and predicted composition of absorption process is used to obtain B_0 and B_1. It is found that reaction between carbon dioxide and MEA is instantaneous, and the axial conversion of carbon dioxide in the gas phase varies exponentially with the contactor length.

1 Introduction

Removal of carbon dioxide has been practiced industrially for several decades. Different processes need to have CO_2 removed. In natural gas processing, CO_2 is removed to reduce the costs of compression, transportation and corrosion. In ammonia manufacture, CO_2 needs to be removed from the hydrogen stream, since it poisons the catalyst for the reaction between H_2 and N_2. Power plant flue gases are a new application of CO_2 removal processes, compared to the first two. In this case, CO_2 is removed only to reduce greenhouse emissions. This issue is of increasing interest, because global warming is an important environmental and political issue. With the Kyoto protocol of 1997, forty-one industrialized countries agreed to cut the carbon dioxide emissions to approximately 5% less than the emissions in 1990, in a five year period going from 2008 to 2012 [1]. This situation makes CO_2 capture an important issue in the economies of most countries. It is a fact that a CO_2 removal facility is an expensive plant, and the operating costs are very high. For a power plant the removal of 90% of the CO_2 from the flue gas can use up to 30% of the energy produced by the plant (IEA Greenhouse Gas R&D Programme) [2]. This represents a heavy loss, and the focus of research in this field is to reduce the costs of removal, in particular reducing its energy requirements. CO_2 has some uses and can be sold on the market. It is used mostly in Enhanced Oil Recovery (EOR). CO_2 flooding represents one of the main methods for extracting the final amounts of recoverable oil from depleted reservoirs. CO_2 is also used in the food industry for carbonated beverages [2]. It finds uses in smaller quantities as inert gas or as supercritical solvent. The problem of the CO_2 market is that many processes produce CO_2 as a by-product, and there is no need to buy from flue gas plants. In addition the amount of CO_2 needed for the aforementioned processes is much smaller than the amount that can be recovered from power

* Corresponding author: e-mail: ghenis@missouri.edu

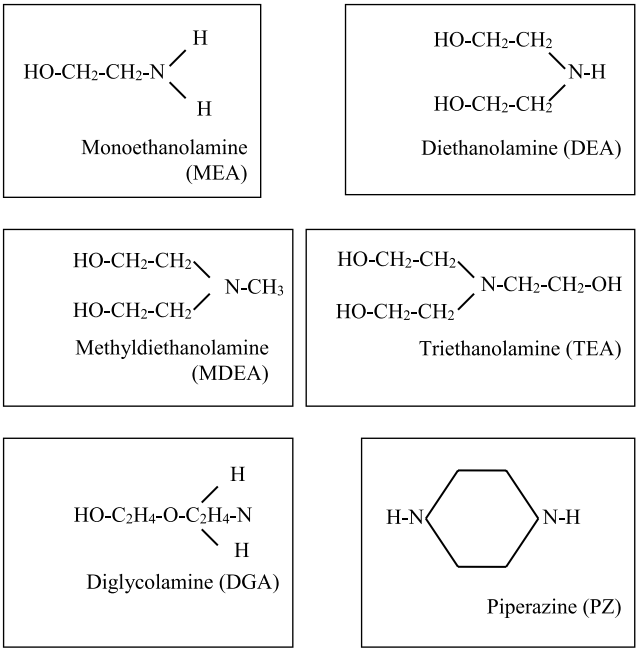

Fig. 1. Chemical structures of most common alkanolamines [1].

plant flue gases. CO_2 capture is typically done by absorption with alkanolamine-water solutions although other processes were also considered such as catalytic hydrogenation [3] and utilization in renewable energy technologies [4]. The alkanolamines are bases, and they react with the acid species CO_2 to form different reaction products. They contain alcohol groups in order to become soluble in water. The first alkanolamine to be used industrially was monoethanolamine (MEA). This is the only amine that will be considered in this work, the chemical structure is shown in Figure 1 compared to the structures of other common alkanolamines, such as methyldiethanolamine (MDEA), diethanolamine (DEA), triethanolamine (TEA), diglycolamine (DGA), and piperazine (PZ). The amines are distinguished as primary, secondary and tertiary, according to the number of organic groups attached to the alkaline nitrogens. MEA is a primary amine, DEA and PZ are secondary amines, and MDEA and TEA are tertiary amines. The different categories of amines differ on the type of mechanisms with which they react with CO_2, as well as the reaction products and the heats of reaction. Typically primary and secondary amines react forming a carbamate species, and the reaction may or may not proceed through an intermediate called the Zwitterions [5].

$$CO_2 + R_2NH \leftrightarrow R_2NH^+COO^- \text{ (zwitterion)}, \quad (1)$$

$$R_2NH^+COO^- + R_2NH \leftrightarrow R_2NCOO^- + R_2NH_2^+ \quad (2)$$

(carbamate)(protonated amine)

Tertiary amines cannot form a carbamate species, because they do not have a hydrogen attached to the nitrogen atom. Typically the tertiary amines react according to equation (3).

$$CO_2 + R_3N + H_2O \leftrightarrow HCO_3^- + R_3NH^+ \quad (3)$$

Primary and secondary amines usually react fast er than tertiary amines, and CO_2 has higher heats of absorption in these amines. Heats of reaction at 25 °C and unloaded conditions are approximately 20.3 kcal/mole for MEA and 14.8 kcal/mole for MDEA [6]. For MEA, the equation is particularly simple. The rate is dominated by the zwitterion formation, rather than by its reaction with another base. The advantage of a fast reacting amine is that the size of the separation equipment (absorbers) is smaller. The drawback is that more heat is required to reverse the reaction and regenerate the solvent. Solvent regeneration is the main obstacle to cost reduction of CO_2 capture. The choice of a proper solvent is important. Some work has been done on mixed solvents. Bishnoi [7] and Dang [8] researched the properties of piperazine promoted MDEA and MEA respectively. Cullinane [9] studied the absorption into piperazine promoted potassium carbonate (K_2CO_3). Piperazine has very fast kinetics and can promote the absorption rates. MDEA, MEA and K_2CO_3 provide CO_2 capacity in the solvent and reduce the heat of regeneration, which would be otherwise too high if piperazine was to be used by itself. These mixed solvents are being studied at bench scale, but they are not yet used in industry. Sharifi and Omidbakhsh Amiri [10] studied the effect of tower type on gas sweetening process. They found that different internals give different efficiency of gas capturing. The first industrial application of the falling film principles was in the form of falling film evaporator [11]. The surprising characteristics of this type of evaporator made the investigators of the field increasingly start to study mass and reaction mechanism through the falling film device, since most absorption and reaction mechanisms are accompanying with a heat transfer process. The falling film device offers greater benefits than the conventional one for many industrial processes, namely [12]:

- It can be operated at low temperature difference between heating medium and liquor.
- Operation is stable at high turndown ratios.
- It can be cleaned more effectively and more efficiently.
- It is more suitable for computer controlled facilities.
- It is more economical to operate and require less operation attention.

Figure 2 shows a sectional view of the falling film contactor, a liquid of the reactant falls by gravity, completely wetting the solid wall and contacting the vapor which is diluted in an inert gas generally air. The solid surface is refrigerated by extremely circulating water. Due to the high surface to volume ratio of liquid in the column, efficient heat elimination takes place. Additional temperature control is achieved by diluting the reactive gas with air or with nitrogen. In some falling film reactors, the control of the film temperature is of considerable importance since by product formation can occur at higher temperature [13]. The engineer in the process industries is usually concerned with the operation of existing plants and the development of new process. In the first case the control, improvement,

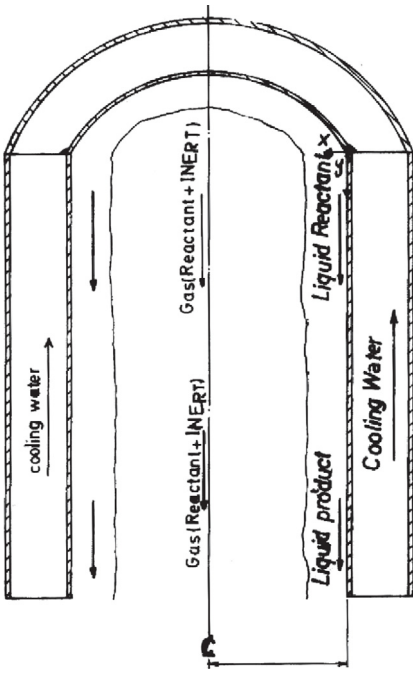

Fig. 2. Sectional view of a falling film contactor.

and optimization of the operation are the engineer's main objectives. In order to achieve this, a quantitative representation of the process, a model is needed which would give the relationship between the various parts of the system. The objective of modeling is to construct, from theoretical and empirical knowledge of a process, a mathematical formulation which can be used to predict the behavior of this process. Thus, mathematical modeling receives high attention in such falling film processes and other sweetening towers [14] to control the process temperature. In order to achieve this goal for CO_2-MEA system, a model is needed to obtain the relationship between the different operating and design parameters of the system for the purpose of industrial design. To validate the mathematical model, experimental measurements of CO_2 absorption by MEA are conducted.

2 Mathematical modeling

The mathematical model consists of differential balance equations in the liquid phase with their corresponding boundary conditions. Through these equations, velocity, concentration, and temperature profiles are obtained. The equations are based on steady state operation, common in industrial and laboratory reactors.

2.1 The principle assumptions

Modeling of the liquid phase is based on the following assumptions:

- The liquid circulates in a laminar flow, and the gas circulates co-currently in a turbulent flow.
- The liquid film is symmetric with respect to the contactor axis.
- The film thickness is small compared to the column radius.
- Liquid reactant and liquid product are assumed to be nonvolatile at working temperatures.
- The solubility of the reactant gas in the liquid reactant and in the reaction product is ideal according to Henry's law.

2.2 Equations of the mathematical model

The column is divided into N number of annular segments as shown in Figure 3. Thus, there are N number of equations for the liquid reactant and the same number of equations is presented for the dissolved gas. To formulate a comprehensive model, the effects of hydrodynamics, mass transfer, kinetics, and heat transfer have to be included.

2.2.1 Hydrodynamics

The liquid shear and velocity profiles are obtained using Navier-Stockes equations, which state that for an element volume of moving fluid, the rate of change of momentum equals the net of the forces acting on the element volume [15] mathematically expressed with respect to Figure 3 as:

Rate of change of momentum per unit volume = viscous force on element per unit volume + pressure force on element per unit volume + gravity force on element per unit volume

$$\rho_l \frac{\partial U_y}{\partial t} = \mu_L \left[\frac{\partial U_y}{\partial x^2} + \frac{\partial^2 U_y}{\partial y^2} + \frac{\partial^2 U}{\partial z^2}\right] - \frac{\partial P}{\partial y} + \rho_L g_g. \quad (4)$$

Which is for steady state one-dimensional flow reduces to:

$$\rho_L g_y - \frac{\partial P}{\partial y} + \mu_L \frac{\partial^2 U_y}{\partial x^2} = 0. \quad (5)$$

Or in the form of shear stress:

$$\rho_L g_y - \frac{\partial P}{\partial y} - \frac{\partial R}{\partial x} = 0. \quad (6)$$

For a constant axial pressure gradient equation (5) becomes:

$$\frac{\partial^2 U_y}{\partial x^2} = -\frac{\Omega}{\mu_L}, \quad (7)$$

where, $\Omega = \rho_L g_y - \frac{\partial P}{\partial y} = \text{constant}$.

The gas phase exerts an interfacial shear R_i on the liquid film, and the velocity varnishes at the solid boundary, so according to Figure 3, we can write the boundary conditions as:

$$\begin{aligned} &\text{At} \quad x = \delta, \frac{\partial U_y}{\partial x} = \frac{R_i}{\mu_L}. \\ &x = 0, \text{Uy} = 0 \end{aligned} \quad (8)$$

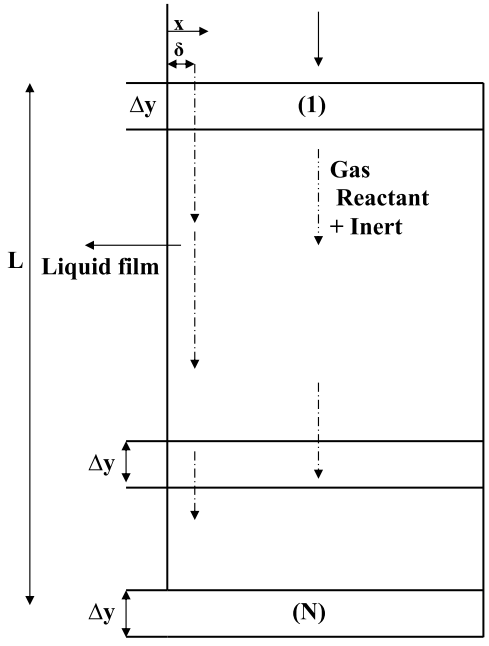

Fig. 3. Falling film contactor divided into N annular segments each of length y and thickness.

Hanratty and Engen [16], Cohen and Hanratty [17], and others have measured interfacial shear in two phase gas–liquid flows, reporting the interfacial friction factor ϕ_i defined by:

$$\varphi_i = \frac{R_i}{\rho_{G.} \cdot U^2{}_G}. \tag{9}$$

Integrating equation (7) twice, and applying boundary conditions, we obtain:

$$\frac{dU_y}{dx} = -\frac{\Omega}{\mu_L}x + C_1. \tag{10}$$

$$U_y = -\frac{\Omega}{2\mu_L}x^2 + C_1 x + C_2. \tag{11}$$

Substitute equation (8) into (11), to obtain, $C_2 = 0$
Substitute equation (9) into (10), to obtain,

$$C_1 = \frac{R_i}{\mu_L} + \frac{\Omega\delta}{\mu_L}. \tag{12}$$

Substitute equation (12) into equation (11) yields:

$$U_y = -\frac{\Omega x^2}{2\mu_L} + \left[\frac{R_i}{\mu_L} + \frac{\Omega\delta}{\mu_L}\right]x,$$

or

$$U_y = \frac{a.x}{\delta} - \frac{b.x^2}{\delta^2}, \tag{13}$$

where

$$a = \frac{R_i\delta + \Omega\delta^2}{\mu_L}, \tag{13a}$$

$$b = \frac{\Omega\delta^2}{2\mu_L}. \tag{13b}$$

Equation (13) presents velocity profile in the liquid film.
To develop an equation describes the shear profile through the liquid film; equations (10) and (12) are used:

$$\frac{dU_y}{dx} = -\frac{\Omega x}{\mu_L} + \frac{R_i}{\mu_L} + \frac{\Omega\delta}{\mu_L} \quad \text{or } \mu_L\frac{\partial U_y}{dx} = \Omega(\delta - x) + R_i. \tag{14}$$

$$R = \Omega(\delta - x) + R_i. \tag{15}$$

At the wall, equation (15) becomes,

$$R_w = \Omega\delta + R_i. \tag{16}$$

The film thickness is obtained from the volumetric flow rate per unit length of wetted perimeter, Q_L, which is related to the velocity distribution by the following equation:

$$Q_L = \int_0^\delta U_y(x)\cdot dx. \tag{17}$$

Substitute equation (13) into equation (17) yields:

$$Q_L = \int_0^\delta \frac{a.x}{\delta} - \frac{b.x^2}{\delta^2}\cdot dx$$
$$Q_L = \delta\cdot\left[\frac{a}{2} - \frac{b}{3}\right]. \tag{18}$$

Substitute equations (13a) and (13b) into equation (18) yields:

$$Q_L = \left[\frac{R_i\delta^2}{2\mu_L} + \frac{\Omega\delta^3}{3\mu_L}\right]. \tag{19}$$

Equation (19) is cubic equation in δ which is readily solved by substituting the numeric values of Q_L, R_i, Ω and μ_L.

To evaluate the interfacial friction factor (ϕ_i), for a turbulent gas, Blasius equation [18] is utilized:

$$\phi_i = E\cdot(0.04)\cdot Re_G^{-0.25}, \tag{20}$$

E is a correction factor introduced by our model to account for the gas entrance effect, since the gas flow in this study is not a fully developed turbulent flow. It is assumed further that E decreases exponentially with the axial distance from the contactor entrance:

$$E = B_0\exp(-B_1 y). \tag{21}$$

The constants B_0 and B_1 are determined later on from the experimental work.

2.2.2 Mass transfer

The general behavior is considered in the mass transfer model, for which the gaseous solute diffuses in the liquid film and then reaction occurred, so the process of diffusion and chemical reaction can still be represented by an extension of the film theory by a method according to Hatta [19]. Thus a zone of reaction between gaseous solute (CO_2) and liquid reactant (MEA), which moves away from the gas–liquid interface taking up some position towards the bulk of the liquid. The final location of this reaction zone will be such that the rate of diffusion of CO_2 from the gas–liquid interface equals the rate of diffusion of MEA from the main body of the liquid.

Figure 4 presents the paths of CO_2, MEA, and liquid product in the liquid form, so CO_2 diffuses through the gas film as a result of driving force ($P_G - Pi$) and diffuses to the reaction zone as a result of equilibrium with Ci. The MEA diffuses from the bulk liquid to the reaction zone under a driving force, q, and nonvolatile product diffuses back to the main bulk of liquid under a driving force (m−n).

2.2.2.1 Concentration profile

To determine the concentration profile, the column is divided into N sections of annular segments as in Figure 3, and a differential (mass or mole) balance equation is applied for each segments. Therefore two differential balances sufficient to determine the concentration profiles, an equation for CO_2 (A component) and the second equation is used for MEA (B component), both in liquid phase. For the element shown in Figure 3, a partial differential element of liquid with dimensions of $\delta x \times \delta y \times 1$ is considered. The amount of the liquid carried in y direction by bulk flow, plus the amount of liquid diffusing in x direction, should be sufficient to maintain the proceeding of the chemical reaction. Symbolically:

$$\text{Input rate} = U_y \cdot C_A \cdot \delta x + [-D_1 \tfrac{\partial CA}{\partial x} \cdot \delta_y]$$

$$\text{Output rate} = U_y . C_A . \delta_x + \tfrac{\partial}{\partial y}(U_y . C_A . \delta_x)\delta_y - D_1 . \tfrac{\partial CA}{\partial x} . \partial y + \frac{\partial}{\partial x}[-D_1 \frac{\partial C_A}{\partial x} . \partial y] . \partial x$$

$$\text{Consumption rate} = r_A \cdot (\delta_x * \delta_x * 1)$$

$$\text{Input rate} - \text{output rate} + \text{consumption rate} = \text{accumulation}$$

$$\text{Accumulation} = 0$$

$$\therefore \text{Input rate} - \text{Output rate} + \text{consumption rate} = 0$$

$$-Uy \frac{\partial C_A}{\partial y} + D_1 \partial^2 \frac{C_{A_A}}{\partial x^2} + r_A = 0. \quad (22)$$

Similarly for liquid reactant (B), the differential balance equation is as follows:

$$-Uy \frac{\partial C_B}{\partial y} + D_2 \partial^2 \frac{C_{B_B}}{\partial x^2} + r_B = 0. \quad (23)$$

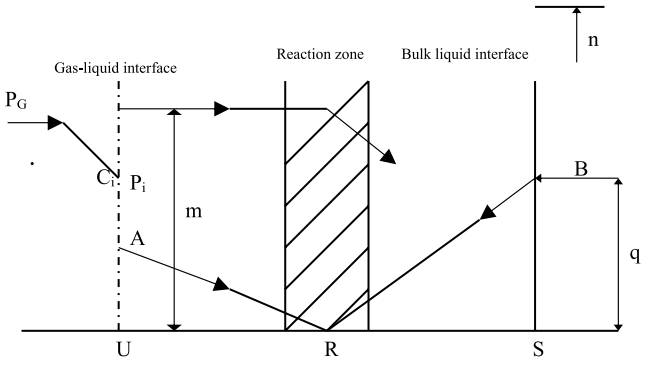

Fig. 4. Absorption with chemical reaction – concentration profiles.

Yih and Liu [20], Yih and Seagrave [21] studied the effect of gas–liquid interfacial shear on mass transfer through the liquid film, and concluded that shear stress induces a greater turbulence in the liquid phase, decreasing its resistance to mass transfer, and eddy diffusion, D_E cannot be disregarded with respect to molecular diffusion. Therefore, any eddy diffusion term, D_E, as a function of the radial coordinate X, is introduced in the microscopic mass transfer, and diffusivities in equations (22) and (23) become,

$$\left.\begin{aligned} D_1 &= D_A + D_E \\ D_2 &= D_B + D_E \end{aligned}\right\}. \quad (24)$$

Rearranging equations (22) and (23) and introduce equation (24) yields:

$$U_y \frac{\partial C_A}{\partial y} = \frac{\partial}{\partial x}\left[(D_A + D_E) \cdot \frac{\partial C_A}{\partial x}\right] + r_A. \quad (25)$$

$$U_y \frac{\partial C_B}{\partial y} = \frac{\partial}{\partial x}\left[(D_B + D_E) \cdot \frac{\partial C_B}{\partial x}\right] + r_B. \quad (26)$$

2.2.2.2 Boundary conditions

Boundary conditions are required to solve equations (25) and (26):

$$y = 0, C_B^0, C_A = 0. \quad (27)$$

$$x = 0 \frac{\partial C_B}{\partial x} = 0, \ \frac{\partial C_A}{\partial x} = 0. \quad (28)$$

$$x = \delta, \frac{\partial C_B}{\partial x} = 0, \ N_A = K_G\left(C_A^G - C_A^{IG}\right), \quad (29)$$

where

$$N_A = -D_A \frac{\partial C_A}{\partial x}. \quad (29a)$$

Equation (28) indicates that the components (A and /or B), mathematically and in fact, cannot pass through the wall. Equation (29) indicates that A crosses the interface at a rate depends on mass transfer of A, and that B is not volatile (assumption number 4 in section 2.1) and cannot cross the interface.

2.2.2.3 *Equilibrium conditions*

(a) Rate of absorption

In the steady state absorption process, the rate of transfer of material through the gas film is the same as that through the liquid film, and the general equation of mass transfer [18] may be written as:

$$N_{CO_2} = \frac{K_{OG}}{R_g T_S}\left[P^G_{CO_2} - P^*_{CO_2}\right], \tag{30}$$

where:

N_{CO_2}: molar flux of gaseous reactant, kmol/m^2.s(CO_2)

K_{OG}: overall gas phase mass transfer coefficient, m/s

R_g: gas–liquid interface temperature, K°

$P^G_{CO_2}$: partial pressure of CO_2 in gas phase, N/m^2

$P^*_{CO_2}$: partial pressure of CO_2 in gas phase which is in equilibrium with bulk liquid phase, N/m^2.

(b) Henry's constant

Danckwerts [22] mentioned that in many cases, so long as the concentration of dissolved gas is small and the temperature and pressure are far removed from the critical temperature and pressure of the gas, Henry's law is obeyed and the concentration C_{CO_2} of dissolved gas is in equilibrium with a partial pressure Pi of the gas as given by

$$P^*{}_{CO_2} = H_e C_{CO_2}, \tag{31}$$

where:

C_{CO_2}: concentration of unreacted CO_2 in solution, kmol/m^3

H_e: Henry's law constant, (N/m^2), m^3/kmol)

If the gas reacts in solution, Henry's law does not apply to the total concentration of unreacted gas.

For the CO_2-MEA system, at the temperature range of 0–60 °C and 6–30% MEA Yunda *et al.* [23] reported the following relation:

$$\ln H_e = 170.7126 - \frac{8477.711}{T_S} - 21.957\ln T_S + 0.00578 T_S, \tag{32}$$

where:

T_S: is the gas–liquid interface temperature (K).

(c) Conversion of CO_2

When CO_2 is absorbed into aqueous MEA solution, the following overall reaction should be considered :

$$CO_2 + 2R_2NH \rightarrow R_2NCOO^- + R_2NH_2^+. \tag{33}$$

The form of the equilibrium constant which was given by Danckwerts and Sharma [24] is:

$$K = \frac{[R_2NCOO^-][R_2NH_2]^+}{[CO_2][R_2NH]^2}. \tag{34}$$

Savage and Kim [25] presented the following relation for the equilibrium vapor pressure of CO_2:

$$P^* = \frac{H_e}{K}\left[\frac{Z}{1-2Z}\right]^2, \tag{35}$$

where:

K: dissociation constant

Alatiqi *et al.* [26] stated the following relation between K and Ts is applicable:

$$\ln K = C_1 + \frac{C_2}{T_S} + C_3 \ln T_S + C_4 T_S. \tag{36}$$

For MEA-CO_2 system

$C_1 = 1.2825$, $C_2 = 3456.179$, $C_3 = C_4 = 0$

Substituting the numeric values of C_1, C_2 and C_3 in equation (36) yields:

$$\ln K = 1.2825 - \frac{3456.79}{T_S}. \tag{37}$$

$$\ln K - 1.2825 = \frac{3456.79}{T_S} \Rightarrow K = \exp\left[1.282 - \frac{3456.179}{T_S}\right]. \tag{38}$$

and equation (32) is rewritten as

$$H_e = \exp\left[89.452 - \frac{2934.6}{T_S} - 11.592\ln T_S\right]. \tag{39}$$

Thus

$$\frac{H_e}{K} = \exp\left[\frac{89.452 - \frac{2934.6}{T_S} - 11.592\ln T_S}{1.282 - \frac{3456.179}{T_S}}\right]. \tag{40}$$

Substituting equation (40) into equation (35) yields:

$$P^* = \exp\left[\frac{89.452 - \frac{2939.6}{T_S} - 11.592\ln T_S}{1.282 - \frac{3456.179}{T_S}}\right] \cdot \left[\frac{Z}{1-2Z}\right]^2. \tag{41}$$

Substituting equation (41) into equation (30) yields

$$N_{CO_2} = \frac{K_{OG}}{R_g T_S}\left[P^G_{CO_2} - \exp\left(\frac{89.452 - \frac{2934.9}{T_S} - 11.59\ln T_S}{1.282 - \frac{3456.17}{T_S}}\right) \times \left(\frac{Z}{1-2Z}\right)^2\right]. \tag{42}$$

Astarita *et al.* [27] observed that up to 20% amine concentration the Vapor Liquid Equilibrium (VLE) remained essentially unchanged. For our experimental conditions the above analysis is used for VLE since the amine concentration varies from 3% to 18% in this study.

To obtain the molar conversion of CO_2 :

$$\text{Conversion} = \frac{N_{CO_2} * A_S}{M_{CO_2}}, \tag{43}$$

where:

A_S: total area of mass transfer, m^2

M_{CO2}: Initial molar rate of CO_2, kmol/s.

2.2.2.4 *Mass transfer coefficients*

(a) Gas-Side Mass Transfer Coefficient

The gas-side mass transfer coefficient is estimated using McReady and Hanratty equation [28]:

$$\frac{k_G}{U^*} = I\cdot(SC)_G^{-0.0704}, \tag{44}$$

where:

k_G: gas-side mass transfer coefficient, m/s

U^*: gas-side interfacial velocity, m/s

$$\text{Sc : Schmidt number} = \left[\frac{\mu}{\rho\cdot D_{CO_2}}\right]_G. \tag{44a}$$

I: a correction term for entrance effect on heat transfer determined later from experimental results.

Yih and Liu [29] defined friction velocity as:

$$U^* = \sqrt{\frac{R_i g_c}{\rho_G}}, \tag{45}$$

where: gc: conversion factor $= \frac{kg\cdot m}{N\cdot sec^2} = 1$

Substitute equation (9) into (45) and rearrange to obtain:

$$\mathrm{U}* = \sqrt{\phi}\mathrm{U}_G \tag{46}$$

Substituting equation (46) into (44) yields:

$$k_G = I\sqrt{\phi_i}U_G(Sc_G)^{-0.0704}. \tag{47}$$

(b) Liquid side mass transfer coefficient

To estimate the liquid side mass transfer coefficient, the correlation of Vivian and Peaceman [30] is used. They investigated the characteristics of CO_2–H_2O system in a wetted wall column and suggested the following equation:

$$\mathrm{K_L} = 0.433\left[\frac{\mu_L}{\rho_L D_A}\right]^{1/2}\left[\frac{g_y L^3}{\mu_L^2}\right]^{1/6}\left[\frac{4\Gamma}{\mu_L}\right]^{0.4} - \frac{D_A}{L}, \tag{48}$$

where:

D_A: diffusion coefficient of solute in liquid, m^2/s

g_y: gravitational constant $= 9.78\,m/sec^2$.

L: length of wetted wall, m.

Γ: mass rate of flow of liquid per wetted length, kg/m.s

μ_L: viscosity of liquid, $N\cdot s/m^2$.

ρ_L: density of liquid, kg/m^2

K_L: liquid-side mass transfer coefficient, m/s

c) Overall mass transfer coefficient

The overall mass transfer coefficient for the absorbed component CO_2 consists of the gas, and liquid side mass transfer coefficients and is expressed as:

$$\frac{1}{K_{OG}} = \frac{1}{K_G} + \frac{H_1}{K_L}. \tag{49}$$

$$H_1 = \frac{H_e}{R_G.T_S}. \tag{50}$$

Substituting equation (49) into equation (42):

$$N_{CO_2} = \mathrm{O}_2^{CO_2}\frac{K_G K_L}{R_G T_S(K_L + H_1 K_G)}$$

$$\left[P_{CO_2}^G - \exp\frac{89.45 - \frac{2934.6}{T_S} - 11.59\ln T}{1.282 - \frac{3456.17}{T_S}}\left(\frac{Z}{1-2Z}\right)^2\right]. \tag{51}$$

2.2.3 Mechanism and rate of reactions

2.2.3.1 *Mechanism of reactions*

Haruo *et al.* [31] suggested the following mechanism for the reaction of MEA-CO_2:

$$CO_2 + 2RNH_2 \Leftrightarrow RNH_3^+ + RNHCOO^- \tag{52}$$

$$CO_2 + RNHCOO^- + 2H_2O \Leftrightarrow RNH_3^+ + 2HCO_3^-, \tag{53}$$

Where R refers to $HOCH_2CH_2$. At very short exposure times of the liquid to the gas encountered in industrial absorber, the effect of reaction 53 can be neglected, and only reaction 52 influences the absorption rate of carbon dioxide [32]. Reaction 52 takes place in two steps:

$$CO_2 + RNH_2 \Leftrightarrow H^+ + RNHCOO^- \tag{54}$$

$$H^+ + RNH_2 \Leftrightarrow RNH_3^+ \tag{55}$$

Danckwerts [33] reported that the equilibrium constants of reactions 54 and 55 are 10^{-5} and 10^{10} l/gmol, respectively. The second step, equation (55), is ionic and instantaneous; whereas the first step, equation (54) is second order, that is first order with respect to carbon dioxide and MEA, and rate controlling. Thus, the overall

reaction 52 is considered as an irreversible, instantaneous and second order reaction with a stoichiometric coefficient of 2 and the equilibrium constant is 10^5 l/gmol. When the absorption of solute gas A is accompanied by an irreversible reaction, the average rate of absorption, NA, is represented by the following equation:

$$N_A = \beta(2\sqrt{D_A/\pi{\cdot}t})A_i. \tag{56}$$

For absorption with a second order reaction of the following stoichiometry:,

$$\mathrm{A} + 2\mathrm{B} \rightarrow \text{Products}$$

The penetration model solution for the reaction factor is closely approximated by the following equation [34]:

$$\beta = (\gamma{\cdot}\eta + \frac{\pi}{8\gamma{\cdot}\eta}){\cdot}erf\left(\frac{2\gamma{\cdot}\eta}{\sqrt{\pi}}\right) + \frac{1}{2}\exp\left(-\frac{4\gamma^2{\cdot}\eta^2}{\pi}\right), \tag{57}$$

η is a dimensionless parameter given by the following equation:

$$\eta = \sqrt{\beta_i/\beta_o} = \sqrt{\beta_\infty - \beta/\beta_\infty - 1}, \tag{58}$$

where β_∞ is the reaction factor for the absorption accompanied with an instantaneous reaction and expressed in terms of σ as follows:

$$\begin{aligned}\beta_\infty &= 1/\mathrm{erf}(\sigma)\\ &\mathrm{erf}(\sqrt{D_A/D_B}\sigma)\exp[(D_A/(D_B-1))\sigma^2].\end{aligned} \tag{59}$$

$$= \sqrt{D_B/D_A})(B_0/2_A)erf(\sigma). \tag{60}$$

2.2.3.2 Rate of reaction

Caplow [35] and Danckwerts [22] suggested that CO_2 reacts with amine to form an intermediate called a "Zwitterion"

$$\mathrm{CO_2} + \mathrm{NR_2H}K2\,K_2\,\mathrm{NR_2HCOO^+}. \tag{61}$$

The Zwitterion can be deprotonated by any base may present in the solution producing a carbamate ion and a protonated base according to the following equation:

$$\mathrm{NR_2H^+COO^-} + \mathrm{B}Kb\,K_b\,\mathrm{NR_2COO^-} + \mathrm{BH^+}. \tag{62}$$

In this study, the homogeneous catalysis mechanism which is developed by Haruo *et al.* [31] is considered. Blauwhoff *et al.* [36] stated that according to this mechanism the rate of the forward reaction in equation (55) is developed based on the assumption of a pseudo steady state conditions for the Zwitteron concentration [7]

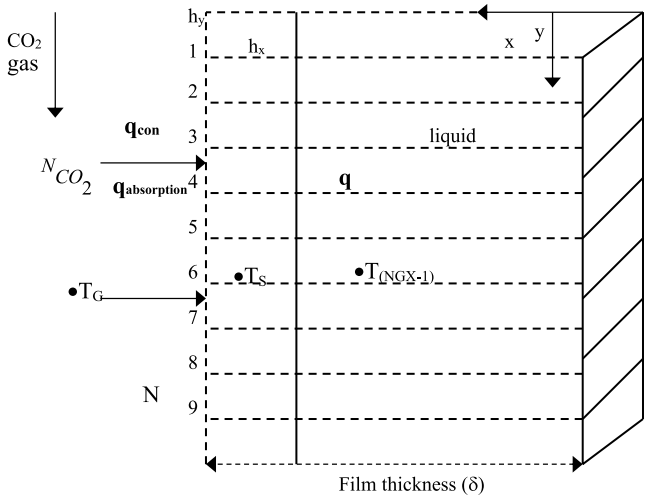

Fig. 5. Mathematical analysis of the interfacial temperature profile.

as follows:

$$r = \frac{k_2[\mathrm{CO_2}][\mathrm{NR_2H}]}{1 + \frac{k_{-1}}{\sum k_b[B]}}. \tag{63}$$

where:

k_b: reaction rate constant for Zwitterion deprotonated, m^3/mol.s

k_{-1}: reverse reaction rate constant, s^{-1}

k_2: second order reaction rate constant, m^3/mol.s

Depending on the relative magnitude of the individual reaction rate constants, different orders and rate constants may obtained with different amines. Values of k_b for various amines (bases) were obtained by Blauwhoff *et al.* [36] and Versteeg and Van Swaaij [37] correlated the rate constant k_2 with liquid temperature and basicity of amines for five different types of amines and obtained the following correlation:

$$\ln k_2 = 16.26 + Pk_b - \frac{7188}{T}. \tag{64}$$

T: temperature, K

2.2.4 Heat transfer

Figure 5 shows a heat balance on a liquid element of dimensions $\delta_x * \delta_y * 1$:

- Heat input by convection + Heat input by conduction:

$$Uy{\cdot}(\delta_x * 1){\cdot}\rho_L{\cdot}C_{PL} + \left[-k_L{\cdot}(\delta_y * 1){\cdot}\frac{\partial T}{\partial x}\right]. \tag{65}$$

- Heat generated

$$-(\delta_x * \delta_y * 1) \times \Delta H_r{\cdot}r_A. \tag{66}$$

Heat input − Heat output + Heat generated = 0

$$-\frac{\partial}{\partial y}\left(U_y{\cdot}\delta_x{\cdot}\rho_L{\cdot}C_{P_L}{\cdot}T\right){\cdot}\delta_y-\frac{\partial}{\partial x}\left(-k_L{\cdot}\delta_y{\cdot}\frac{\partial T}{\partial x}\right){\cdot}\delta_x +(-(\delta_x{\cdot}\delta_y{\cdot}\Delta H_R{\cdot}r_A))=0. \quad (67)$$

Dividing by δ_x .δ_y and rearranging yields:

$$U_y{\cdot}\frac{\partial}{\partial y}\left(\rho_L C_{P_L}T\right)=-\frac{\partial}{\partial x}\left(-k_L\frac{\partial T}{\partial x}\right)-\Delta H_R{\cdot}r_A. \quad (68)$$

Equation (68) is used to develop the temperature profile through the column.

2.2.4.1 Boundary conditions

Boundary conditions are required to solve equation (68):

$$\mathrm{y}=0,\mathrm{T}=\mathrm{T}_0. \quad (69)$$

$$\mathrm{x}=0,\frac{\partial T}{\partial x}=0. \quad (70)$$

$$\mathrm{x}=\delta,k_L\frac{\partial T}{\partial x}=h_G{\cdot}(T_G-T_{x=\delta}), \quad (71)$$

where:

T_G: temperature of the gas, °K

h_G: gas heat transfer coefficient, W/m^2.°K

Condition b is based on the assumption that the column is well insulated from ambient while condition c assumes that heat transfers from the liquid to the gas.

2.2.4.2 Gas-side heat transfer coefficient

Bird *et al.* [15] stated that the solutions of many mass transfer problems at low mass transfer rates can be obtained by analogy with corresponding problems in heat transfer. Based on this principles, Mc Ready and Hanratty [28] introduced the following equation for gas side heat transfer coefficient:

$$h_G=P\sqrt{\phi_i}{\cdot}U_G{\cdot}(P_{rG})^{-0.0704}{\cdot}\rho_G{\cdot}C_{PG}, \quad (72)$$

where:

P_{rG}: Prandtle number of gas side, $\left(\frac{C_P\mu}{k}\right)_G$

k: Gas thermal conductivity, W/m.°K,

C_P: heat capacity of gas,

μ: dynamic viscosity of gas,

Referring to Figure 5, the heat flux q into the liquid is the sum of heat conducted across the gas film ($q_{cond.}$) and heat of absorption which is proportional to the molar flux of solute into the liquid at the interface[N_{CO_2}], symbolically speaking:

$$-k_L\frac{\partial T}{\partial x}=h_G{\cdot}(T_G-T_S)+(-\Delta H_S){\cdot}N_{CO_2}(J), \quad (73)$$

where:

ΔH_S: heat of absorption of CO_2 in MEA, kJ/kmol.

$NCO_2(J)$: molar flux of CO_2 into the liquid at segment J of the contactor, kmol/m^2.s

(J): 1, 2,....N

N: no. of annular segments of liquid film along the contactor

Using finite difference operator to approximate the differential operator, equation (73) becomes:

$$-\frac{k_L}{h_x}[T_{NGX-1}-T_S]=h_G{\cdot}(T_G-T_S)+(-\Delta H_S){\cdot}N_{CO_2}(J).$$

Solving for T_S

$$T_S=\frac{h_G{\cdot}T_G+T_{(NGX-1)}{\cdot}\frac{k_L}{h_x}+(-\Delta H_S){\cdot}N_{CO}(J)}{\left[h_G+\frac{k_L}{h_x}\right]}, \quad (74)$$

where:

h_x: grid spacing in x-direction, m.

$T_{NGX\text{-}1}$: Liquid temperature at distance h_x from T_S, K

N_{GX} : grid points in x-direction

Substitute equation (NCO_2) 51 in equation (74) yields:

See equation 75 below page

where:

$$\mathrm{A}=\frac{h_G.T_G}{\left[h_G+\frac{k_L}{h_x}\right]},\mathrm{G}=\exp\frac{89.45-\frac{2934.6}{T_S}-11.59\ln T_S}{1.282-\frac{3456.17}{T_S}}\left(\frac{Z}{1-2Z}\right)^2,$$

$$\mathrm{B}=\frac{k_L.h_x}{\left[h_G+\frac{k_L}{h_x}\right]},\mathrm{C}=\frac{(-\Delta H_S){\cdot}K_{OG}{\cdot}P_{CO_2G}}{R_g{\cdot}\left[h_G+\frac{k_L}{h_x}\right]},$$

$$\mathrm{E}=\frac{(-\Delta H_S).K_{OG}.G}{R_g.\left[h_G+\frac{k_L}{h_x}\right]}$$

To obtain TS, applying Newton-Raphson method on equation (75) yields:

$$T_S=\frac{h_G{\cdot}T_G+T_{(NGX1)}{\cdot}\frac{k_L}{h_x}+(H_S){\cdot}\left[\frac{k_Gk_L}{R_G{\cdot}T_S(k_L+H_1k_G)}\left(P^G_{CO_2}G\right)\right]}{\left[h_G+\frac{k_L}{h_x}\right]}$$

$$T_S=\mathrm{A}+\mathrm{B}{\cdot}T_{NGX1}+\frac{C}{T_S}\frac{E{\cdot}e^{\frac{W}{T_S}}}{T_S}, \quad (75)$$

$$F = 0 = T_S = A - B{\cdot}T_{NGX-1} - \frac{C}{T_S} + \frac{E{\cdot}e^{-\frac{W}{T_S}}}{{T_S}^2}. \tag{76}$$

Derivation of equation (74) w.r.t T_S gives:

$$\frac{dF}{dT_S} = D = 1 - 0 - 0 - \frac{C}{{T_S}^2} + E\left(\frac{W{\cdot}e^{-\frac{W}{T_S}}}{{T_S}^3} - \frac{e^{-\frac{W}{T_S}}}{T_S^2}\right). \tag{77}$$

$$T_S = T_S - \frac{F(T_{S0})}{D(T_{S0})} + \frac{E{\cdot}e^{-\frac{W}{T_S}}}{{T_S}^2}. \tag{78}$$

where:

T_{S0}: the initial estimate of T_S

Equation (78) is the general formula of Newton-Raphson iteration method for obtaining the constants of equation (76). Equations (76), (77), and (78) are used in the computer main program to estimate the interfacial gas–liquid temperature.

2.3 Solution of the mathematical model

Equations (24), (25) and (68) are two dimensional second order nonlinear partial differential equation include:

$$C_A = f(x, y)$$

$$C_B = F(x, y)$$

$$T = S(x, y)$$

Through the liquid film, where *f*, *F* and *S* are functions of two independent variables (*i.e.*, x and y). The above equations cannot be solved analytically. So this is done numerically.

2.3.1 Concentration profiles

Concentrations profiles of CO_2 are obtained by applying the implicit finite difference multigrid method developed by Wesseling [38]. This method implies the solution of N equations (N being the number of annular segments) of CO_2 component and the same number of equations for the amine component. The systems are solved by matrix calculus. For example, to solve equation (24) by the multigrid method, one needs to calculate the coefficients of the differential equation and the parameters of its boundary conditions; such as U_y, D_E, D_A, D_B, h_G, K_G, etc.

2.3.2 Velocity profiles

In order to obtain the velocity profiles given by equation (13), the shear at the gas-side interface, R_i, is given by equation (9). This value is related to the friction factor, φ_i, by equation (20). The film thickness, δ, is calculated from 19 by iteration.

2.3.3 Estimation of model parameters

The developed mathematical model has three parameters, B_0, B_1, and I, whose numerical values are unknown. They must be estimated using experimental data. The problem of fitting the model to experimental data is to find the best value of the parameters that will predict absorption rates of CO_2 which are as close as possible to the experimental values. To develop a comprehensive mathematical model, a mass and an energy balance are conducted on the first annular segment and the outputs from those calculations are used as inputs of the second segment. Mass and energy balance are then conducted on the second segment and so on down the contactor. Velocity profile, film thickness, and physical properties of the materials are estimated for the first segment before applying the balances, but are adjusted for the next segment according to the output temperature and mass flow from each previous segment. This method of calculation gives concentration and temperature profiles in the liquid film of the contactor. The mathematical model developed has the predictive capability to calculate the radial profiles versus contactor height, as well as longitudinal profiles of conversion and temperatures.

3 Experimental work

This part of the study is carried out to obtain experimental data on the absorption reaction of CO_2 in aqueous solutions of MEA. Air stream containing CO_2 enters at the top of contactor and flows downward co-currently with the aqueous MEA solution. The alkaline solution flows downward through the absorber, and leaves at the bottom of the column. The contactor was designed and installed to operate at different ranges of gas and liquid flow rates. All the heat evolved was transferred to the cooling water which flows in a counter current mode through the shell side. Variation in temperature of inlet liquid was small and can be neglected. Furthermore, the temperature of liquor feed was controlled externally to give a temperature within the range of 25–60 °C (± 2 °C). In this study, four parameters are used to obtain concentration and temperature profiles namely, mole fraction of carbon dioxide in gaseous mixture (Y) 0.05, 0.075, and 0.1, molar concentration of absorbent

Table 1. Specification of ex perimental apparatus.

Item number	Description
T-1	Feed tank, 200 L capacity 700*4*637 mm
T-1	Product and regeneration tank 200 L capacity 700*4*637 mm
FA-101	Falling film absorber (mono tube reactor 1")
CY-1,2	CO2 cylinders
FI-1	MEA solution flow meter (1–50 L/hr)
FI-2	Air flow meter (orifice type) (0–50) m3/hr
FI-3	CO2 gas flowmeter (0–7.44) m3/hr
FI-4	Cooling water flowmeter (2.5–55 L/min)
H-1,2	Electrical heaters of tank T-102 (7000 watt) each, type B, manufacturer Britain
P-1	MEA solution pump, monotype, flow 1.5 m^3/hr, head: 10 m, 750 rpm, driven by electrical motor
M-1	Gases mixer 4 in diameter, 20 cm packed with stainless steel gauze

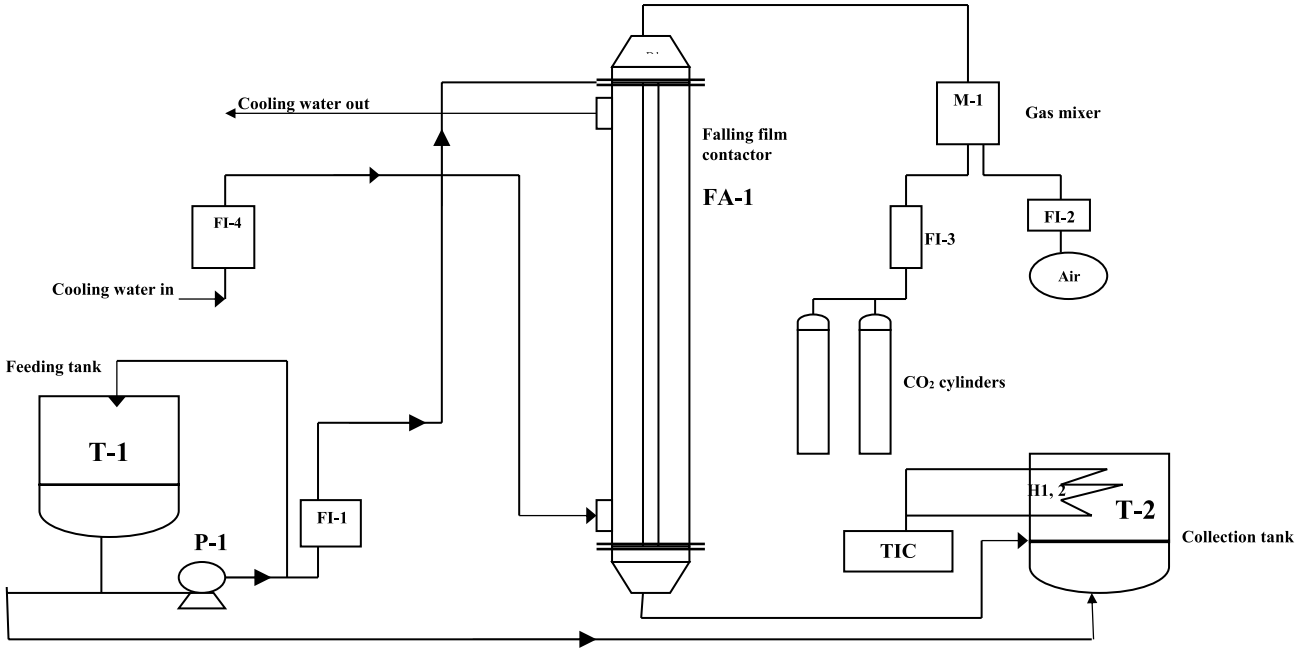

Fig. 6. A flow diagram of the experimental apparatus.

(monoethanolamine) (C_{MEA}) 1, 2, and 3 M, volumetric flow rate of MEA (Q_{MEA}) 5, 10, 15 and 20 L/hr, and temperature of MEA (T) 30, 35, 40, 45, 50, and 55 °C.

3.1 Materials

Carbon dioxide is supplied as 20 kg cylinder and air is supplied via an air compressor. Monoethanol amine, chemical indicators and reagents are supplied by *Sigma Aldrich*. The specifications of all gases and chemicals used in this study are presented in Table 1.

3.2 Apparatus and procedure

A schematic flow diagram of the experimental apparatus is shown in Figure 5. The main part of this apparatus is the monotubular falling film contactor. The liquid and gas streams are introduced to the reactor at the required temperature. The liquid MEA is introduced at the top of the column section through a pan distributor made of stainless steel. Hobler *et al.* [39] showed many different types of liquid distributor for wetting vertical tubes internally. He reviewed their dimensions and operating conditions. In this study a distributing device was used for uniform wetting of tube at a low degree of wetting. This distributor was presented by Kharisov and Kogan [40]. It is characterized by simplicity in design and wetting intensity is within the liquid loading condition of the present experimental runs. Basically, it consists of a cylindrical pan with 46 holes (1.0 mm diameter) drilled in the base. The gas was introduced 30 mm below the falling section using spherical distributor of 30 mm diameter, which gives good gas distribution. Carbon dioxide is fed through a regulator and rotameter (FI-1) and mixed with air (supplied by an air

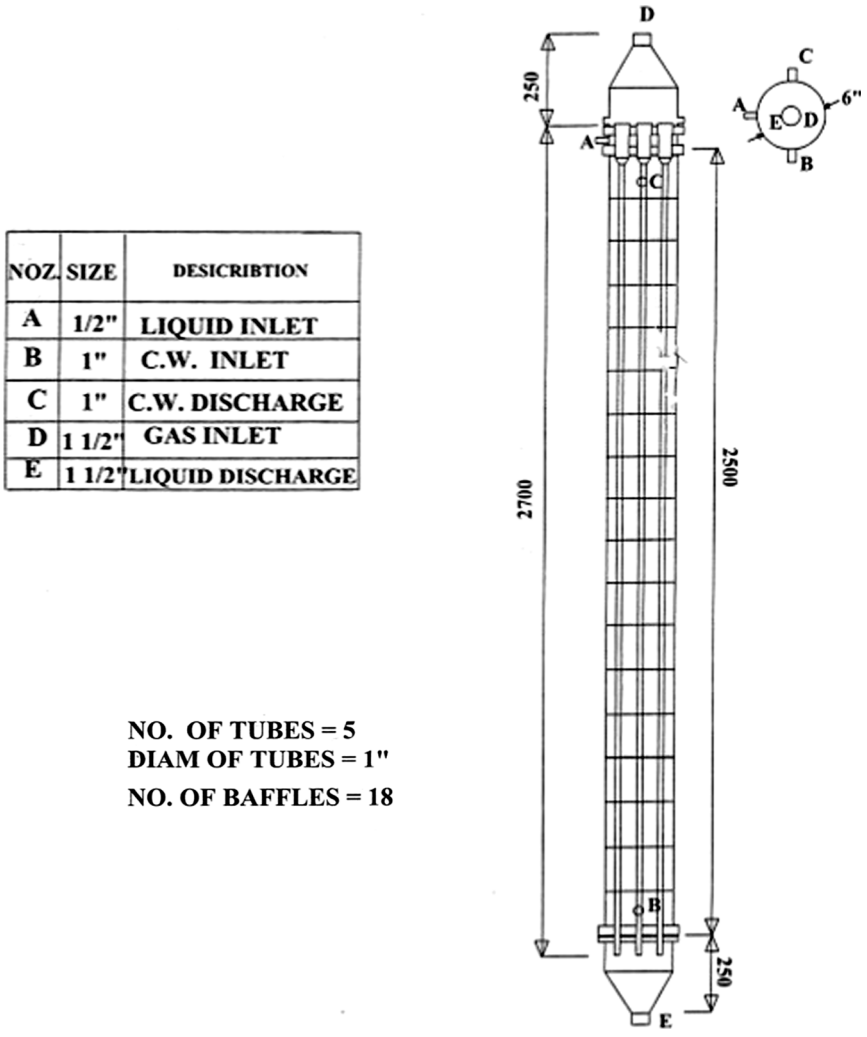

Fig. 7. The monotube contactor.

Table 2. Specification of chemicals used.

No.	Item	Specificatio n	Qt.
1	Monoethanolamine	Liquid state purity 99.65 % (supplier: Northern refinery Com. Baiji, purity was analyzed using UV- spectrophotometer)	200 Lt
2	Carbon dioxide	Purity 99.5 % (manufacturer : Iraqi Soft drink Com., purity was analyzed using Gas chromatography, Shimadzo-9A)	10 cylinders
3	Air	Compressed	
4	HCl, $BaCl_2$	Supplier: Fluka (Germany)	500 gm
5	Methyl orange phenolphthalein	Supplier: Fluka (Germany)	200 ml 200 ml

compressor) in a homogenizing mixer to obtain a mixture at the desired concentration, to flow co-currently with the liquid downwards the contactor. The mixer is a cylindrical stainless steel box filled with a stainless steel gauze packing. The inlet section, before the falling film zone, is long enough to humidify the gas mixture with the amine solution. The temperatures of the gas and liquid are measured at the inlet and the outlet of the contactor. The temperature of the gas feeding stream was kept approximately constant at 35 °C ± 2 °C using a temperature controller. The absorption column is made of stainless steel AISI 316L tube of nominal diameter 1 in (ANSI B36.19); actual inner diameter 0.0223 m, with a wall thickness of 3 mm, the length of the contactor is 2.5 m. The absorber is supplied

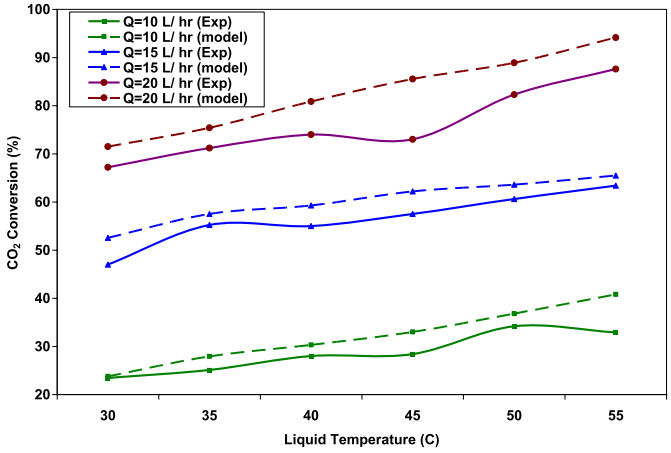

Fig. 8. CO_2 conversion vs. liquid temperature for different liquid flow rates at constant mole.

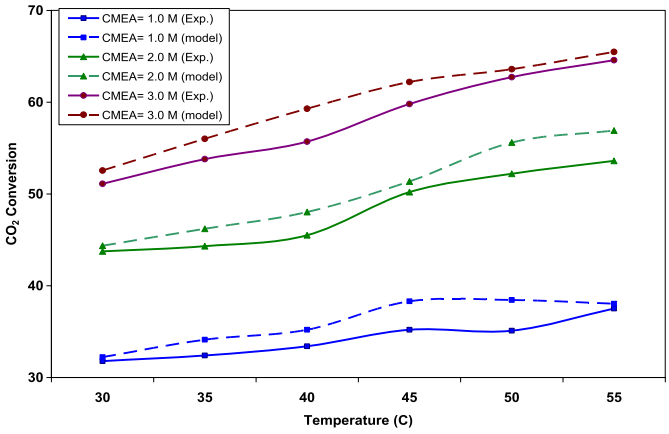

Fig. 9. CO_2 conversion *vs.* liquid temperature for different liquid concentration at constant liquid.

with a cooling jacket, for the purpose of exothermic reactions to be performed. The dimensions of the implanted design are shown in Figure 7. The outlet solution goes to a regeneration tank (200 L), where liquid samples are collected for analysis at the entrance of the tank. The total amine concentration in the collected solution is found by titration with 0.1 N HCl to the end point of methyl orange as an indicator. To determine free amine content in presence of carbonate, the latter precipitated with excess of 10% $BaCl_2$ and titrated with 0.1 N HCl using phenolphthalein as an indicator. To calculate the amount of carbon dioxide absorbed, m, 5 ml of the collected solution is titrated with 0.1 N HCl against methyl orange as an indicator.

Consumption of 0.1 N HCl = a ml. A second 5 ml sample of collected solution of a second liquor sample is added to 20 ml $BaCl_2$ solution. After 10 min, the sample is titrated with 0.1N HCl using phenolphthalein as an indicator. Consumption of 0.1 N HCl = b ml [41].

The amount of CO_2 absorbed is:

$$\frac{(a-b)*2.2}{5*44} = \text{m M } CO_2/\text{ml MEA}. \quad (79)$$

A computerized UV- spectrophotometer (Jasco 520, manufacturer Jasco, Japan) is used to measure the concentration of MEA solution. Specifications of the devices and control elements are presented Table 2.

4 Results and discussion

The operating conditions and the experimental CO_2 conversions are fed to a MatLab code programed based on the models developed in section 2. A predicted CO_2 conversion is obtained and plotted versus the experimental conversion with a 3.978 % standard error. This statistical function gives a first cross check for the reliability of the developed model since the limitation of acceptance for the standard error test is 10%. To observe the behavior of the developed model at different operating conditions compared to the experiment results, carbon dioxide conversion is considered as a criteria of comparison.

4.1 Effect of MEA temperature

Reaction temperature has a significant effect on conversion. With an increase in MEA reaction temperature, the rate of chemical reaction increases and viscosity of the solution decreases, which leads to an increase in absorption rate and consequently CO_2 conversion. These results are in agreement with Thomas [42], Maddox [43], and Abid [44]. Figure 8 shows the impact of MEA temperature on CO_2 conversion in MEA solution at different liquid flow rates, constant mole fraction of CO_2 (Y = 0.1) and constant absorbent concentration (3 M). The same trend is observed in Figure 9 at different liquid concentrations, at Y = 0.075 and constant liquid flow rate (Q = 15 L/hr). The highest conversion is obtained at 3 M and 20 L/hr MEA compared to the minimum conversion obtained at a 1 M and 10 L/hr.

4.2 Effect of mole fraction of carbon dioxide in gas phase

Experimental and predicted results show a proportional relation between mole fraction of carbon dioxide and CO_2 conversion, starting from 0.05 to 0.1, this behavior is shown in Figure 10 and are in agreement with the results of Hikita *et al.* [45], Tontiwachwuthikul *et al.* [46] and Abid [44].

4.3 Effect of MEA concentration

Figure 11 shows the impact of MEA concentration on the conversion of CO_2 at different MEA flow rates, constant MEA temperature (T = 55 °C) and constant mole fraction of carbon dioxide (Y = 0.1). It shows a good reliability of the predicted conversion with the experimental results. The highest conversion is obtained at the same liquid concentration (*i.e.*, of 3 M MEA), which in line with

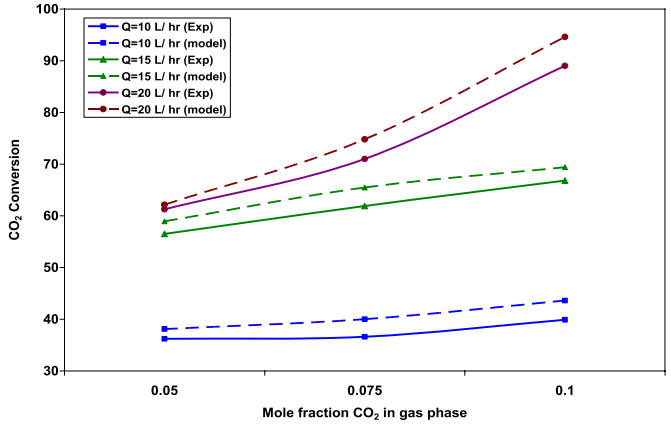

Fig. 10. CO_2 conversion *vs.* mole fraction of CO_2 in gas phase for different liquid flow rates at constant liquid concentration (3 M) and at constant liquid temperature (T = 55 °C).

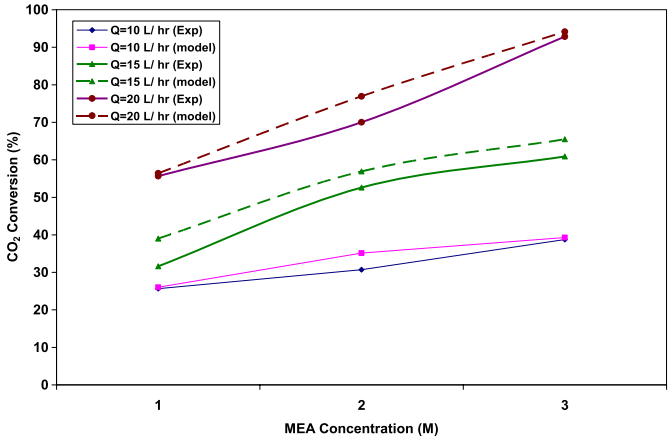

Fig. 11. CO_2 conversion vs. liquid concentration for different liquid flow rates at constant liquid temperature (T = 55 °C) and constant CO_2 mole fraction ($Y = 0.1$).

relevant literature [6,47,48]. Studies of Abid [44], Hitchcock and Cadot [49] and Maloney [50] showed that there is a critical of CO_2 conversion appears upon running at a progressive increase of amine concentration, then it falls to an equilibrium conversion. This behavior can be attributed to following fact, as increasing of MEA concentration can give more chances for the reaction to be occurred, also there is an observed increase in MEA viscosity that results in an additional resistance to solute diffusion.

4.4 The developed model

4.4.1 Validation of the developed model

To verify the validity of the developed model, standard error has been determined for the results plotted in Figures 8 through 11 at different operating conditions. Table 3 presents the standard errors obtained accordingly at a 95% confidence level. It is seen that all the standard errors obtained are acceptable (less than 10%). Herby, the developed is reliable.

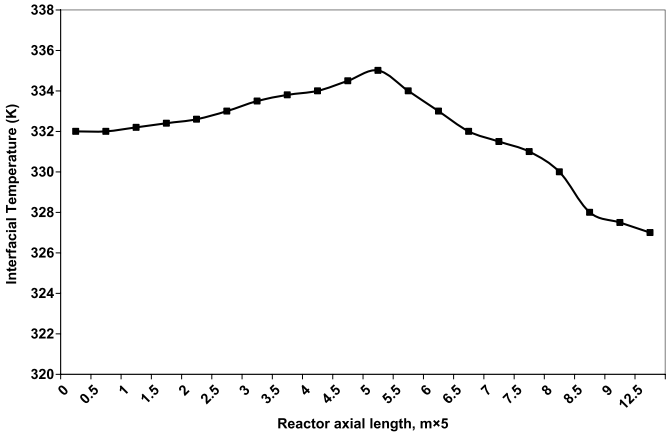

Fig. 12. Interfacial temperature profile along the contactor length as predicted by present model for CO_2 fraction 0.1, QL = 20 L/hr and CMEA = 3 M.

4.4.2 Results of the developed model

The present model is developed to predict radial and axial velocity, concentration, and temperature profiles through the liquid falling-film along the contactor. The axial conversion of the solute in the gas phase and the axial interfacial temperature can be also predicted. A trial experiment ($Y = 0.1$, $Q_L = 20$ L/hr and T = 55 °C) is used as an input condition to the developed model.

4.4.2.1 Interfacial temperature profile

Figure 12 shows the interfacial temperature along the contactor predicted by the model. It is seen that the average increase of interfacial temperature is 3 K through the first meter of the contactor while cooling effect of the gas stream becomes obvious after the first meter and diminishes the interfacial temperature lower than the initial input temperature of liquid.

4.4.2.2 Concentration distribution

The present model has the capability to predict concentration profile of the reactants through the liquid film, axially and radially. Figures 13 and 14 show a linear surface distribution of free CO_2 in the liquid film and the radial distribution of CO_2 along the contactor. The concentration profiles indicate that the reaction between CO_2 and MEA is instantaneous which is consistent with Davis [51] theory. Figure 15 shows a surface distribution of free amine concentration in the liquid film and Figure 16 shows the radial distribution of free amine in the liquid film at different mole fractions of CO_2. They indicate that the present model described the effect of amine in liquid solutions from the viewpoint of homogeneous catalysis mechanism theory [18]. This theory states that the chemical reaction is fast and mass transfer processes are limited in a small region close to the gas–liquid interface due to the bulk flow of amine, named boundary layer. Thus, the $CO_2 + MEA$ reaction is fast enough that CO_2

Table 3. Statistical Comparison between the present model and experimental results.

Figure	Liquid flow Q_L L/hr	Liquid conc. M	Present Model vs. Experimental % Standard error
8	10		4.56
	15		3.24
	20		2.37
9		1	2.87
		2	2.54
		3	1.72
10	10		7.21
	15		4.36
	20		3.68
11	10		4.35
	15		3.74
	20		2.62

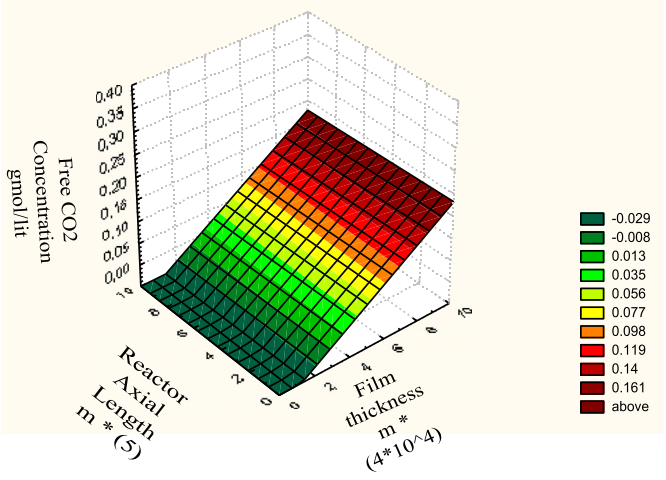

Fig. 13. Surface distribution of free CO_2 concentration in the liquid film for CO_2 fraction 0.1, QL = 20 L/hr and CMEA = 3 M as predicted by present model.

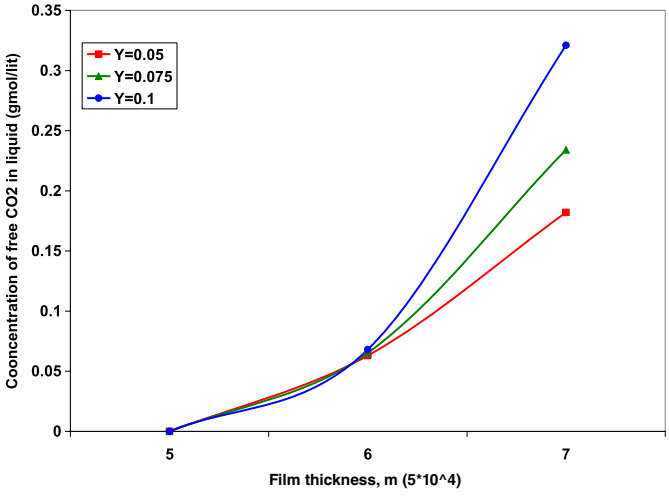

Fig. 14. Radial distribution of free CO_2 in liquid film for CO_2 fraction 0.1, QL = 20 L/hr and CMEA = 3 M as predicted by present model.

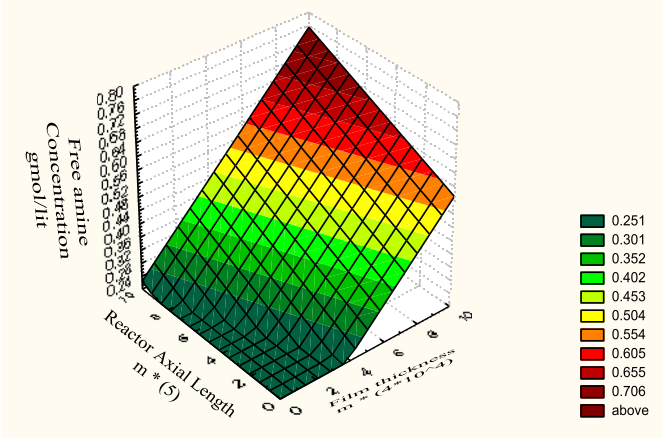

Fig. 15. Linear surface distribution of free amine concentration through the liquid film along the contactor for CO_2 fraction 0.1, QL = 20 L/hr and CMEA = 3 M.

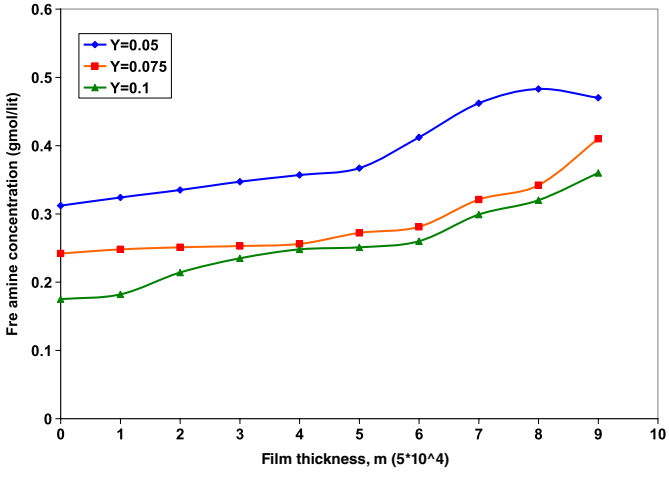

Fig. 16. Radial distribution of free amine concentration in liquid film at different distances contactor entrance for CO_2 fraction 0.1, QL = 20 L/hr and CMEA = 3 M.

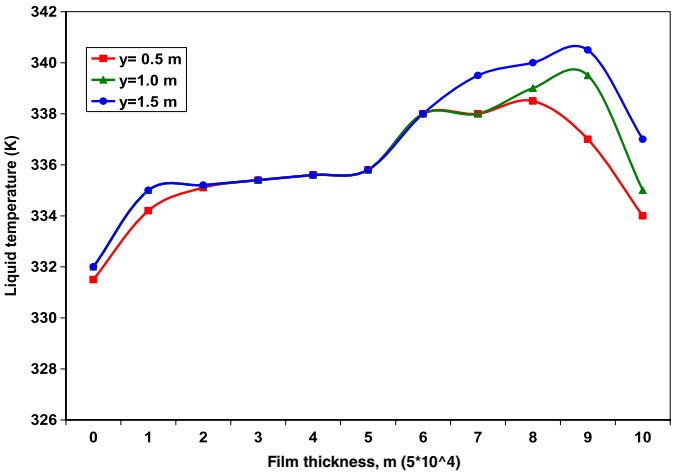

Fig. 17. Radial distribution of liquid temperature at different distances contactor entrance for CO_2 fraction 0.1, QL= 20 L/hr and CMEA = 3 M.

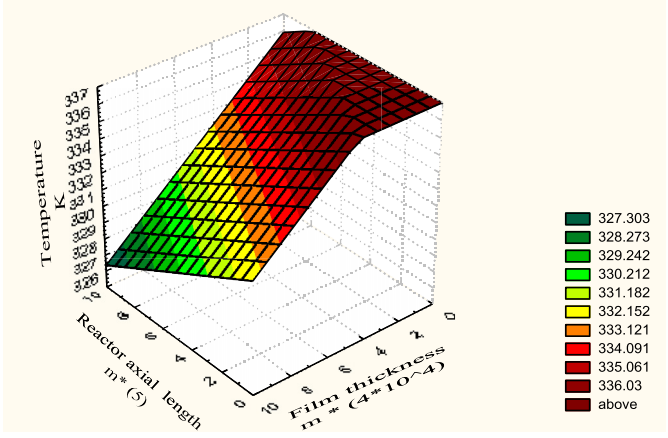

Fig. 18. Linear surface distribution of temperature through the liquid along the contactor.

approaches equilibrium with the other components of the solution at its interface composition. This is consistent with King [52] theory. Also it is seen in Figure 15 that the assumptions of insignificant depletion of MEA at the interface and the reaction products do not build up at the interface are confirmed and the concentrations of every component in the solution, except CO_2, can be considered constant in the liquid boundary layer.

4.4.2.3 Temperature distribution

Figure 17 presents the radial distribution of liquid temperature at different heights from the contactor entrance. Figure 18 presents linear surface distribution of liquid temperature along the contactor. The following observations can be noticed from these figures:

– The liquid temperature distribution presents a typical bulge shape. This is due to the fact that the exothermic reaction produces heat and the heat is absorbed by the liquid and gas streams. This means that the liquid absorbs most of the heat in the top of the contactor.

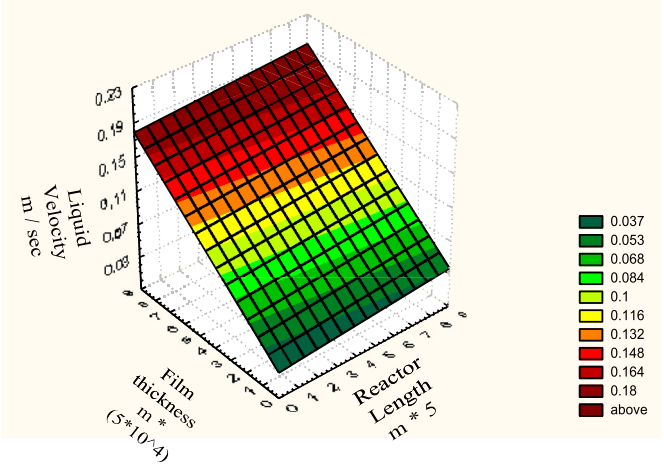

Fig. 19. Surface distribution of liquid velocity.

– At constant CO_2 content in gas stream, the liquid flow in the column is relatively small, thus the liquid heat capacity is small. As a consequence, the liquid temperature gradient at the top of the absorber is very steep. Even though the reaction occurs throughout the column, the temperature starts to decrease in the middle of the column, because the liquid is cooled by the flue gas flowing up the column till a constant value of temperature.
– The average increase of liquid temperature along the first meter of the contactor length is within 2 K.

4.4.2.4 Velocity distribution

Figure 19 presents the linear surface distribution of liquid velocity along the contactor. It can be seen from equation (6) that the maximum liquid velocity is obtained at the gas–liquid interface and the minimum value (*i.e.*, Uy = 0) is obtained at tube wall, equation (6) is utilized the present model to predict velocity profile in the liquid film along the contactor. The parameters influences velocity profile are gas flow rate, liquid flow rate, liquid viscosity, and tube wall roughness. Liquid velocity is proportional to gas and liquid flow rate while it is inversely proportional to liquid viscosity and tube wall roughness.

4.4.2.5 Equilibrium concentrations

The present model is capable in predicting the equilibrium concentrations of free amine, carbamate, protonated amine, carbonate, hydroxyl and hydrogen ions for each experimental run. Starting with given values of MEA molarity and amine conversion in solution, one can calculate the equilibrium concentrations of ions for hydrogen, hydroxyl, carbonate, bicarbonate, protonated amine and free amine according to the following equations:

$$H_2OKW \leftrightarrow^{K_W} H^+ + OH^-. \quad (80)$$

$$HCO_3^- KW \leftrightarrow^{K_W} H^+ + CO_3^=. \quad (81)$$

$$[OH^-] = \frac{K_W}{K_2} \cdot \frac{[CO_3^=]}{HCO_3^-}. \quad (82)$$

They defined the carbonate conversion (x_0) as moles CO_2 absorbed per mole MEA, chemically expressed as:

$$x_0 = \frac{[HCO_3^-] - [OH^-]}{K^+}. \quad (83)$$

And the hydroxyl ion concentration was derived as a simple function of the carbonate conversion(x_0):

$$[OH^-] = \frac{K_W}{K_2} \cdot \frac{1 - x_0}{2x_0}, \quad (84)$$

K_W m K_2 are equilibrium constant given by Kent and Eisenberg [53] as a function of temperature. Now, if we substitute equation (84) into equation (83) and rearranging yields:

$$x_0 = \frac{[HCO_3^-] - \frac{K_W}{K_2} \cdot \frac{1-x_0}{2x_0}}{K^+}$$
$$[HCO_3^-] = x_0[K^+] + \frac{K_W}{K_2} \cdot \frac{1 - x_0}{2x_0} \quad (85)$$

Substituting equations (83) and (84) into equation (81) and rearranging yields:

$$\frac{K_W}{K_2} \cdot [CO_3^=] = [OH^-] \cdot [HCO_3^-]$$
$$= \frac{K_W}{K_2} \cdot \frac{1 - x_0}{2x_0} \cdot \left(x_0 \cdot [K^+] + \frac{K_W}{K_2} \cdot \frac{1 - x_0}{2x_0} \right) [CO_3^=]$$
$$= \frac{1 - x_0}{2x_0} \cdot \left(x_0[K^+] + \frac{K_W}{K_2} \cdot \frac{1 - x_0}{2x_0} \right). \quad (86)$$

Protonation of amine

$$RNH_2^+ Ka \leftrightarrow^{Ka} H^+ + RNH. \quad (87)$$

Carbamate hydrolysis is expressed as follows:

$$RNHCO_2^- + H_2O K3 \leftrightarrow^{K_3} RNH + HCO_3^-. \quad (88)$$

Apply electro neutrality yields:

$$[K^+] + [H^+] + [RNH_2^+] = [OH^-] + 2[CO_3^=] + [HCO_3^-] + [RNCO_2^-]. \quad (89)$$

Apply a material balance yields:

$$[RNH]_0 = [RNH^+] + [RNH] + [RNCO_2^-]. \quad (90)$$

Apply equilibrium on equations (81) and (87) and combine yields:

$$R^+ = \frac{K_2}{K_a} \cdot R \cdot \frac{HCO_3^-}{CO_3^=} = \frac{K_2}{K_a} \cdot R \cdot \frac{2x_0}{1 - x_0}. \quad (91)$$

Combine equation (87) and (88) to obtain H^+:

$$H^+ = \frac{K_a}{K_5} \cdot \frac{R^+}{R^-} . HCO_3. \quad (92)$$

Combine equation (89) and (90) yields:

$$R^- = R_T - R - \frac{K_2}{K_a} \cdot R \cdot \frac{2x_0}{1 - x_0}. \quad (93)$$

Substitute equations (91) and (93) into equation (92) yields:

$$H^+ = \frac{K_2}{K_3} \cdot R \cdot \left(\frac{2x_0}{1 - x_0} \right) \cdot \frac{HCO_3^-}{\left[R_T - R - \frac{K_2}{K_a} . R \left(\frac{2x_0}{1-x_0} \right) \right]}. \quad (94)$$

Substitute equations (91), (93) and (92) into equation (89) yields:

$$\frac{A_1 . R}{(R_T - R - A_2 . R)} + A_2 \cdot R = A_3 - R - A_2 \cdot R, \quad (95)$$

where:

$$A_1 = \frac{K_2}{K_3} \cdot \left(\frac{2x_0}{1 - x_0} \right) \cdot HCO_3. \quad (96)$$

$$A_2 = \frac{K_2}{K_a} \cdot \left(\frac{2x_0}{1 - x_0} \right). \quad (97)$$

$$A_3 = OH^- + 2HCO_3^= + HCO_3^- - K^+ + RT. \quad (98)$$

Simplifying equation (95) and put $\frac{K_2}{K_3} = 0$ yields:

$$(3A_2^2 + 3A_2) \cdot R^2 - (A_2 \cdot A. + 2RT \cdot A_2 + R_T) . R + R_T \cdot A_3 = 0. \quad (99)$$

Equation (99) is a quadratic equation in R and can be solved easily as follows:

$$R = \frac{W \pm \sqrt{W2 - 4.V \cdot Z}}{2Z}. \quad (100)$$

where: $W = (A_2 + 1) . A_3 + R_T . (2A_2 + 1)$, $V = RT \cdot A_3$ $Z = 3A_2 (1 + A_2)$

By successive substitution of equation (100) into equations (93), (91) and (92), the numeric values of R^-, H^+, and R^+ are estimated as shown in Table 4. The predicted concentrations indicate a proportional relationship between concentration of bicarbonate ion and carbonate conversion. The concentration of hydroxyl ion is inversely proportional to carbonate conversion. Other concentrations of ions like free amine, carbamate, protonated amine, and carbonate are expressed chemically by equations (84), (85), (86), (91), (93) and (94) respectively.

Table 4. Equilibri um concentration of ions as predicted by the present model.

Run No.	Free MEA	RNH_3^+	$RNHCOO^-$	OH *10^5	$HCO3^-$	CO_3^{-2} *103
1	0.125	0.0731	0.721	5.94	0.0105	1.62
3	0.113	0.0682	0.638	41.23	0.0091	1.57
3	0.108	0.0532	0.576	3.852	0.00831	1.462
4	0.1062	0.0461	0.523	3.261	0.00771	1.373
5	0.1061	0.0453	0.516	3.13	0.00752	1.323
6	0.1058	0.0426	0.5013	3.082	0.00731	1.310
7	0.123	0.0712	0.704	4.681	0.0101	1.461
8	0.1121	0.0657	0.630	4.031	0.00836	1.437
9	0.1031	0.053	0.541	3.612	0.00731	1.382
10	0.0106	0.042	0.528	3.421	0.00711	1.217
11	0.1054	0.0431	0.484	3.119	0.00684	1.104
12	0.103	0.0417	0.426	3.011	0.00571	1.091
13	0.1042	0.0361	0.495	3.072	0.00665	1.432
14	0.1027	0.0360	0.4873	3.067	0.00635	1.381
15	0.1006	0.0212	0.416	3.028	0.00581	1.273
16	0.0871	0.0193	0.386	2.916	0.00501	1.116
17	0.0812	0.0126	0.351	2.621	0.00446	1.017
18	0.0783	0.0119	0.324	2.416	0.00415	0.934
19	0.1062	0.0612	0.617	4.236	0.00986	1.487
20	0.1031	0.0571	0.5613	4.010	0.00971	1.394
21	0.0972	0.0534	0.528	3.906	0.0086	1.267
22	0.0881	0.0461	0.516	3.761	0.00823	1.109
23	0.0863	0.0423	0.486	3.412	0.00764	1.036
24	0.0813	0.0392	0.4511	3.23	0.00745	1.018
25	0.211	0.0683	0.686	4.435	0.00964	1.411
26	0.208	0.0671	0.673	4.168	0.00920	1.367
27	0.195	0.065	0.661	4.081	0.0087	1.315
28	0.187	0.0613	0.653	4.062	0.00831	1.121
29	0.183	0.0608	0.634	4.051	0.00716	1.105
30	0.232	0.0581	0.621	3.916	0.00709	1.091
31	0.2691	0.0631	0.6670	4.321	0.0088	1.406
32	0.181	0.0622	0.642	4.106	0.00806	1.353
33	0.173	0.0583	0.613	3.812	0.00771	1.3212
34	0.1641	0.0524	0.582	3.738	0.00652	1.273
35	0.634	0.0517	0.572	3.676	0.00634	1.186
36	0.613	0.0504	0.562	3.637	0.00548	1.107

4.4.3 Dependency of model parameters on experimental operating conditions

The present model has three parameters in equation (21). They are predicted for each experiment and tabulated in Table 5. The model parameter E, which is introduced for compensation of gas entrance effect on gas phase heat transfer coefficient, has the following behavior with operating conditions:

- An average increase of carbon dioxide mole fraction by 33.5% results in an average increase of parameter value by 2.24%. This model behavior is due to the fact that the increase in concentration gradient of carbon dioxide gas results in an increase in absorption rate.
- An average increase of the liquid flow rate by 46.7% results in an average increase of parameter value 22.6%. This model behavior results from the inversely thickness of the liquid film which means more resistance to heat transfer.
- An average increase of liquid temperature by 24.5%, results in an average increase of parameter value by 62.5%. This model behavior is due to the fact that the positive temperature gradient between liquid and gas has predominant effect on heat transfer and in improving gas solubility.

Table 5. Model parameters estimated by minimization technique.

Exp.	E	B_0	B_1	CO_2 Conversion
1	0.0628	169.1157	1.2784	28.53
2	0.06354	169.115	1.27884	29.75
3	0.06821	169.114	1.27885	33.75
4	0.06942	169.1021	1.27887	34.42
5	0.07357	169.1002	1.279	36.75
6	0.07319	169.10001	1.279	37.51
7	0.08368	96.7415	0.0274	42.72
8	0.086842	96.6903	0.275503	45.75
9	0.08739	96.6675	0.2752	47.24
10	0.08795	96.6732	0.27512	50.68
11	0.08542	96.6721	0.275041	53.74
12	0.08423	96.345	0.2734	56.85
13	0.08675	54.1958	0.0821	51.47
14	0.0871	54.2004	0.082036	54.1
15	0.08861	53.204	0.08175	57.82
16	0.09325	53.2047	0.0817	60.74
17	0.09364	53.1048	0.08091	61.35
18	0.09674	53.0214	0.08073	63.04
19	0.06427	168.767	1.32585	31.78
20	0.06545	167.916	1.2985	33.65
21	0.06571	167.009	1.29938	34.71
22	0.06623	167	1.29938	36.43
23	0.06744	167.01	1.29952	37.91
24	0.06728	166.924	1.3121	37.51
25	0.08416	92.7415	0.0274	43.75
26	0.08647	91.6903	0.275503	44.31
27	0.08716	90.6675	0.2752	47.36
28	0.08724	86.132	0.27512	50.65
29	0.08852	91.4721	0.275041	54.83
30	0.08865	90.345	0.2734	56.12
31	0.08453	57.5001	1.06927	51.83
32	0.08752	57.621	1.0713	55.23
33	0.09034	57.923	1.0718	58.46
34	0.09254	58.01	1.0732	61.34
35	0.09378	58.123	1.0826	62.72
36	0.0976	58.261	1.0835	64.57

– The amine concentration has a positive effect on the model parameter, for the range of (1–3) M MEA, the model parameter has an average increase of 18.6%.

5 Conclusion

The mathematical model developed for the absorption process of CO_2 gas by MEA solution in a falling film contactor is able to reproduce some plant data, if a correction is applied to the kinetics of the CO_2+MEA reaction obtained from the experimental results. The model uses kinetics to represent the mass transfer in the absorber. The following findings are concluded:

– The adjusted kinetics are based on falling film contactor experiments. The validity of the model is closely related to the quality and accuracy of those data. More tubes in the falling film absorber data would allow for the regression of a more reliable rate constant.
– The mass transfer in the absorber can be controlled by gas phase resistance. The correlation of Yunda *et al.* [54] for K_G is empirical, thus it is accurate for a specific flow range.
– The entrance effect of the falling film contactor can be related to the axial distance from the reactor entrance exponentially.
– The reaction between CO_2 and MEA is instantaneous, since the reaction takes place at the interface [55,56].

– The axial conversion of carbon dioxide in gas phase varies exponentially with reactor length.
– The mathematical model describes the effect of the process variables, liquid temperature, liquid concentration, liquid flow rate, and CO_2 mole fraction in gas phase, on absorption rate of CO_2 in MEA solution.
– The highest concentration of MEA solution, 3 M, is efficient in absorption than the lower one (1 M) successively, this is consistent with the recent researchers trend line in using high concentration of MEA solution range 2–5 M.

Van der Geer, J., Hanraads, J.A.J., Lupton, R.A., 2010. The art of writing a scientific article. J. Sci. Commun. 163, 51–59.

Nomenclature

a_{GL}	gas–liquid interfacial area, m^2/m^3
a_{LS}	liquid–Solid interfacial area, m^2/m^3
b	Stoichiometric coefficients (−)
C_{Ag^*}	equilibrium concentration of gaseous reactant in liquid phase, kmol/m^3
C_{Bi}	concentration of liquid reactant in liquid phase, kmol/m^3
Cb	bulk concentration of active species, kmol/m3
C_{ni}	liquid-phase concentration of species i, kmol/m3
C_i	concentration of species i, kmol/m^3
C_{max}	maximum concentration as reference, w/m^2 K
c_p	specific heat capacity, J/kmol K
D_{AA}	self diffusivity of component A, m^2/s
D_{AB}	molecular diffusivity, m^2/s
d_e	equivalent particle diameter, m
d_h	hydraulic diameter, m
d_p	particle diameter, m
F_{Ao}	molar feed rate of component A, kmol/s
g	gravitational acceleration, m/s2
h_p^G	gas-particle heat transfer coefficients, J/m^2 s K
h_p^G	liquid-particle heat transfer coefficients, J/m^2 s K
h_w^G	gas-wall heat transfer coefficients, J/m^2 s K
h_w^L	liquid-wall heat transfer coefficients, J/m2 s K
h_w^f	fluid-wall heat transfer coefficients, J/m^2 s K
ΔHRi	heat of ith reaction, kJ/mol
ΔHR_{298}	heat of formation, kJ/mol
$KH_{2GL}a_{GL}$	gas–liquid mass transfer coefficient, 1/s
KH_{2GS}	gas–solid mass transfer coefficient, m/s
KH_{2LS}	liquid-solid mass transfer coefficient, m/s
KL_s	apparent liquid-solid mass transfer coefficient, m/s
K_{niLS}	liquid–solid mass transfer coefficient of species i, m/s
k_f	fluid thermal conductivity, J/m s K
k_G	gas thermal conductivity, J/m s K
k_L	liquid thermal conductivity, J/m s K
k_i	reaction rate constant, m^3nkmol1-n/kgcatalyst.h
k_s	liquid–solid mass transfer coefficients, m/s
M_{wt}	molecular weight, kg/kg mol
m	Henry's law constant, atm/(kmol solute/kmol solution)
N	number of experiments (−)
N_a	molar flux of A, kmol/m^2s
P	pressure, MPa
ΔP_i	pressure drop, MPa
$\Delta P/Z$	pressure drop per unit length bed, MPa/m
Q_G	volumetric gas flow rate, m^3/s
Q_L	volumetric liquid flow rate, m^3/s
R	universal gas constant, m^3atm/mol K
r	intrinsic reaction rate, kmol/kgcatalyst.h
r_A	observed reaction rate, kmol/kgcatalyst.h
r_{isj}	intrinsic reaction rate of species i on j the catalyst part (wet or dry section), kmol/kgcatalyst.h
T	reaction Temperature, K
T_o	inlet feed temperature, K
T_f	fluid temperature, K
T_G	gas phase temperature, K
T_L	liquid phase temperature, K
T_R	reference temperature, K
T_r	reduced temperature, K
T_w	wall temperature, K
U_G	superficial gas velocity, m/s
U_L	superficial liquid velocity, m/s
u_f	superficial fluid velocity, m/s
Mwt	molar volume, m^3/kmol
Δx_A	conversion of component A,
Y	axial coordinate, m
Z	reactor length, m

Greek Symbols

α	dimensionless reactant concentration (−)
β_{nc}	dynamic or darning liquid saturation (−)
β_e	external liquid saturation (−)
β_t	Total liquid saturation (−)
γ	reactant limitation criteria (−)
μ	viscosity, kg/m.s
ρ	density, kg/m^3
σ_L	surface tension, N/m

Subscript

ava	average value
G	gas
L	liquid
f	fluid (liquid or gas phase)

Superscript

G	gas
L	liquid
ni	reaction order
1	main reaction
2	side reaction

Dimensionless group

$_{Fr}$ Froude number, $\frac{U_L^2}{gd_e}$

$_{GaL}$ modified Galileo number, $\frac{\rho_L^2 u_p^2 g\varepsilon^3}{\mu_L^2(1-\varepsilon)^3}$

Pr Prandtl number, $\frac{c_p\mu}{k_f}$

R_e Reynold number, $\frac{\rho_L u_L d_e}{\mu_L}$

$R_{'e}$ modified Reynold number, $\frac{\rho_L u_L d_e}{\mu_L(1-\varepsilon)}$

R_{ef} modified Reynold number, $\frac{\rho_L u_L d_p}{6\mu_L(1-\varepsilon)S_f}$

R_e modified Reynold number, $\frac{\rho_L u_L d_e}{\mu_L \varepsilon_{LT}}$

sc Schmidt number, $\frac{\mu}{D_{AB}\rho}$

References

1 Frequia S. (2002) Modeling of CO_2 removal from flue gases with monoethanolamine, *MSc thesis* in Chemical Engineering, The University of Texas at Austin.

2 Garcia Camacho F., Molina Grima E., Chisti Y. (2004) Mixing in bubble column and airlift reactors, *Chem. Eng. Res. Des.* **82**, 1367–1374.

3 Tursunov O, Kustov L, Kustov A. (2017) A brief review of carbon dioxide hydrogenation to methanol over copper and iron based catalysts, *Oil Gas Sci. Technol. – Rev. IFP Energies nouvelles* **72**, 30.

4 Passalacqua R., Centi G., Perathoner S. (2015) Solar production of fuels from water and CO_2: perspectives and opportunities for a sustainable use of renewable energy, *Oil Gas Sci. Technol. – Rev. IFP Energies nouvelles*, 70, 5, 799–815.

5 Al-Baghli N.A., Pruess S.A., Yesavage V.F., Selim M.S. (2001) A rate-based model for the design of gas absorbers for the removal of CO2 and H2S using aqueous solutions of MEA and DEA, *Fluid Phase Equilib.* **185**, 31–43.

6 Kohl A.L., Nielsen R.B. (1997) *Gas Purification*, 5th edition, Houston.

7 Bishnoi S. (2000) *Carbon dioxide absorption and solution equilibrium in piperazine activated methyldiethanolamine, PhD. Dissertation*, The University of Texas at Austin.

8 Dang H. (2001) CO_2 Absorption Rate and Solubility in Monoethanolamine/Piperazine/Water, *MSc Thesis*, The University of Texas at Austin.

9 Cullinane J.T. (2005) Thermodynamics and kinetics of aqueous piperazine with potassium carbonate for carbon dioxide absorption, *PhD Dissertation*, The University of Texas at Austin.

10 Sharifi A., Omidbakhsh Amiri E. (2017) Effect of the tower type on the gas sweetening process, *Oil Gas Sci. Technol. – Rev. IFP Energies nouvelles* **72**, 24.

11 Wiegand J. (1971) Falling-film evaporators and their applications in the food industry, *J. Appl. Chem. Biotechnol.*, **21**, 12, 351–358.

12 Murray A.J. (1986) Practical and economic benefits of falling film evaporation, Plant/Oper. Prog. **5**, 1, 31–34.

13 Akanksha Pant K.K., Srivastava V.K. (2007) Modeling of sulphonation of tridecylbenzene in a falling film reactor, *Math. Comput. Modell.* **46**, 9, 1332–1344.

14 Bashipour F., Rahimi A., Khorasani S.N., Naderinik A. (2017) Experimental optimization and modeling of sodium sulfide production from H_2S-Rich Off-Gas via response surface methodology and artificial neural network, *Oil Gas Sci. Technol. – Rev. IFP Energies nouvelles* **72**, 9.

15 Bird R., Steward W., Lightfoot E. (1960) *Transport phenomena*, Wiley, New York.

16 Hanratty T., Engen J.M. (1957) Interaction between a turbulent air stream and a moving water surface, *AIChE J.* **3**, 299.

17 Cohen L., Hanratty T. (1965) Generation of waves in the concurrent flow of air and a liquid, *AIChE J.* **11**, 138.

18 Coulson J. Richardson J. (1983) *Chemical Engineering*, Vol. 1, 3rd Edition, Pergamon Press, England.

19 Hatta S. (1932) Technol, Repts, Tohoku Imp, Univ., 10, 119.

20 Yih S.M., Liu J.L. (1983) Prediction of heat transfer in turbulent falling liquid films with or without interfacial shear, *AIChE J.* **29**, 903–909.

21 Yih S.M., Seagrave R.C. (1978) Hydrodynamic stability of thin liquid films flowing down an inclined plane with accompanying heat transfer and interfacial shear, *AIChE J.* **24**, 5, 803–810.

22 Danckwerts P.V. (1979) The reaction of CO_2 with ethanolamines, *Chem. Eng. Sci.* **4**, 34, 443–446.

23 Yunda, Liu, Luzheng Zhang, Watansiri S. (1999) Representing vapor−liquid equilibrium for an aqueous MEA−CO_2 system using the electrolyte nonrandom-two-liquid model, *Ind. Eng. Chem. Res.* **38**, 2080–2090.

24 Danckwerts P.V., Sharma M.M. (1966) Absorption of carbon dioxide into solutions of alkalis and amines, The Chemical Engineer CE, 244–280.

25 Savage D.W, Kim C.J. (1985) Chemical kinetics of carbon dioxide reactions with diethanolamine and diisopropanolamine in aqueous solutions, *AIChE J.* **31**, 296.

26 Alatiqi I., Sabri M.F., Bouhamra W., Alper E. (1994) Steady −State Rate −based modeling for CO2/Amine absorption desorption systems, *Gas Sep. Purif.* **4448**, 1, 3–11.

27 Astarita G., Marrucci G., Gioia F. (1964) The influence of carbonation ratio and total amine concentration on carbon dioxide absorption in aqueous monoethanolamine solutions, *Chem. Eng. Sci.* **19**, 95–103.

28 Mc Ready FM., Hanratty T. (1984) In gas transfer at water surface, Reidel D., Dardrecht S. (eds), Holland.

29 Yih S.M. (1987) Modeling heat and mass transfer in wavy and turbulent falling liquid films, *Heat and Mass Transfer*, **21**, 6, 373–381.

30 Vivian S., Peaceman W. (1956) Liquid-side resistance in gas absorption, *AIChE J.*, **2**, 4, 437–443.

31 Haruo H., Satoru A., Yoshio K. (1979) Absorption of carbon dioxide into aqueous monoethanolamine solutions, *AIChE J.* **25**, 5, 793–800.

32 Sada E., Kamazawa H., Butt M.A. (1976) Chemical absorption kinetics over a wide range of contract time: absorption of carbon dioxide into aqueous solutions of monoethanolamine, *AIChE J.* **22**, 1, 196–198.

33 Danckwerts P.V. (1967) The absorption of carbon dioxide into aqueous amine solutions and the effects of catalysis, *Trans. Inst. Chem. Eng.* **45**, T32.

34 Hikita H., Asai, S. (1964) Gas absorption with (m,n) th order irreversible chemical reaction, *Int. Chem. Eng.* **4**, 332–340.

35 Caplow M. (1968) Kinetics of carbamate formation and breakdown, *Am. Chem. Soc.* **90**, 24, 6795–6803.

36 Blauwhoff P.M.M., Versteeg G.F., Van Swaaij W.P.M. (1983) A study on the reaction between CO_2 and alkanolamines in aqueous solutions, *Chem. Eng. Sci.*, **38**, 1411–1429.

37 Versteeg G.F., Van Swaaij W.P.M. (1988) Solubility and diffusivity of acid gases CO2 and N2O in aqueous alkanolamine solutions, *Chem. Eng. Sci.* **43**, 573–585.

38 Wesseling P. (1982) *Multigrid Method*, Springer-Verlag, Berlin.

39 Hobler T., Bandrowski J., Hartland S. (1996) Mass Transfer and Absorber, P.R.P., Warszawa.

40 Kharisov M.A., Kogan V.B. (1967) A distributing device for thin-film evaporation equipment, *Int. Chem. Eng.* **7**, 189–190.

41 Luma J.S. (1996) *Absorption of carbon dioxide by sodium hydroxide and monoethanolamine solution in a packed column, MSc Thesis*, University of Technology, Iraq.

42 Thomas W.J. (1966) The absorption of carbon dioxide in aqueous monoethanolamine in a laminar jet, *AIChE J.* **12**, 1051–1057.

43 Maddox R.N. (1984) *Gas and Liquid Sweetening. Gas Conditioning and Processing, 3rd ed., Norman, OK, Campbell Petroleum Series*, John M. Campbell & Co.

44 Abid M.F. (2002) *Mathematical model and experimental measurement in a falling film reactor, Ph.D Thesis*, University of Technology.

45 Hikita H., Asai S., Ishikawa H., Honda M. (1977) The kinetics of reactions of carbon dioxide with monoethanolamine, diethanolamine and triethanolamine by a rapid mixing method, *Chem. Eng. J.* **13**, 1, 7–12.

46 Tontiwachwuthikul P., Meisen A., Lim C.J. (1992) CO_2 absorption by NaOH, monoethanolamine and 2-amino-2-methyl-1-propanol solutions in a packed column, *Chem. Eng. Sci.* **47**, 381–390.

47 Wen Long C., Kouichi H., Ze Shae C., Atsushi A., Peng H., Takao K. (2004) Heat transfer enhancement by additive in vertical falling film absorption of H_2O/LiBr, *Appl. Therm. Eng.* **24**, 281–298.

48 Weibin C., Yujun W., Shenlin Z. (2005) Flow and mass transfer characteristics in a falling-film extractor using hollow fiber as packing, Chem. Eng. J. **108**, 161–168.

49 Hitchcok J.A., Cadot S.D. (1989) Rate of absorption of carbon dioxide, *Chem. Eng. Sci.*, **8**, 211.

50 Pereira Duarte S., Barreto G.F., Lemcoff N. (1984) Comparison of two-dimensional models for fixed bed catalytic reactors, *Chem. Eng. Sci.*, **39**, 1017–1024.

51 Davidson J.F. (1957) The determination of diffusion coefficient for sparingly soluble gases in liquids, *Trans. Inst. Chem. Eng.* **35**, 51.

52 King C.J. (1966) Turbulent liquid phase mass transfer at a free gas–liquid interface, *Ind. Eng. Chem. Fund.* **5**, 1, 1–8.

53 Kent R.L., Eisenberg B. (1976) Better data for amine treating, *Hydrocarbon Process.* **12**, 87.

54 Yunda, Liu, Luzheng Zhang, Watansiri S. (1999) Representing vapor-liquid equilibrium for an aqueous MEA-CO_2 system using the electrolyte nonrandom-two-liquid model, *Ind. Eng. Chem. Res.* **38**, 2080–2090.

55 Putta K.R, Svendsen H.F, Knuutila H.K (2017) CO_2 absorption into loaded aqueous MEAsolutions: impact of different model parameter correlations and thermodynamic models on the absorption rate model predictions, *Chem. Eng. J.* **327**, 868–880.

56 Aboudheir A., Tontiwachwuthikul P., Chakma A., Idem R. (2003) Kinetic of the reactive absorption of carbon dioxide in high CO_2-loaded, concentrated aqueous monoethanolamine solutions, *Chem. Eng. Sci.* **58**, 5195–5210.